SANDIA REPORT

SAND2004-6004
Unlimited Release
Printed November 2004

Laboratory Evaluation of Damage Criteria and Permeability of Big Hill Salt

Moo Y. Lee, Brian L. Ehgartner, Byoung-Yoon Park and David R. Bronowski

Prepared by
Sandia National Laboratories
Albuquerque, New Mexico 87185

Sandia is a multiprogram laboratory operated by Sandia Corporation,
a Lockheed Martin Company, for the United States Department of Energy's
National Nuclear Security Administration under Contract DE-AC04-94AL85000.

Issued by Sandia National Laboratories, operated for the United States Department of Energy by Sandia Corporation.

Available to DOE and DOE contractors from
U.S. Department of Energy
Office of Scientific and Technical Information
P.O. Box 62
Oak Ridge, TN 37831

Telephone: (865) 576-8401
Facsimile: (865) 576-5728
E-Mail: reports@adonis.osti.gov
Online ordering: http://www.doe.gov/bridge

Available to the public from
U.S. Department of Commerce
National Technical Information Service
5285 Port Royal Rd.
Springfield, VA 22161

Telephone: (800) 553-6847
Facsimile: (703) 605-6900
E-Mail: orders@ntis.fedworld.gov
Online order: http://www.ntis.gov/help/ordermethods.asp?loc=7-4-0#online

SAND 2004-6004
Unlimited Release
Printed November 2004

Laboratory Evaluation of Damage Criteria and Permeability of Big Hill Salt

Moo Y. Lee[1], Brian L. Ehgartner[2], Byoung-Yoon Park[3] and David R. Bronowski[1]

[1]-Geomechanics Department
Sandia National Laboratories
P.O. Box 5800
Albuquerque, NM 87185-0751

[2]-Geotechnology and Engineering Department
Sandia National Laboratories
P.O. Box 5800
Albuquerque, NM 87185-0706

[3]-Performance Assessment and Decision Analysis Department
Sandia National Laboratories
P.O. Box 5800
Albuquerque, NM 87185-1395

ABSTRACT

To establish strength criteria of Big Hill salt, a series of quasi-static triaxial compression tests have been completed. This report summarizes the test methods, set-up, relevant observations, and results. The triaxial compression tests established dilatant damage criteria for Big Hill salt in terms of stress invariants (I_1 and J_2) and principal stresses ($\sigma_{a,d}$ and σ_3), respectively:

$$\sqrt{J_2}\,(psi) = 1746 - 1320.5 \exp^{-0.00034 I_1\,(psi)}$$

$$\sigma_{a,d}\,(psi) = 2248 + 1.25\ \sigma_3\,(psi)$$

For the confining pressure of 1,000 psi, the dilatant damage strength of Big Hill salt is identical to the typical salt strength ($\sqrt{J_2}$ = 0.27 I_1). However, for higher confining pressure, the typical strength criterion overestimates the damage strength of Big Hill salt.

ACKNOWLEDGEMENTS

The authors would like to appreciate the support of Robert E. Myers, DOE SPR PMO FE-4421 who has supported the laboratory experimental project of Big Hill salt. The authors also thank to David Borns and Larry Costin for their managerial support of this report.

Table of Contents

Figures

Tables

1. Introduction

Sandia Geomechanics Department carried out a series of mechanical / hydrological tests of Big Hill salt. The test-matrix consists of triaxial compression tests and permeability measurements before and after the Big Hill salt specimen went through dilatant damage. The objective of this study was to provide dilatant damage criteria and coupled permeability of the salt under quasi-static compressive loading conditions so that the 3-D modeling effort could predict the safety factor and the standoff distance for a cavern in the Big Hill SPR (Strategic Petroleum Reserve) site (Park *et al.*, in preparation). This report summarizes the test methods, set-up, relevant observations, and results from our experimental efforts.

The Big Hill SPR site shown in Figure 1 has been the subject of investigations resulting in significant engineering, testing, and analysis programs in recent years. The investigations include those related to gas intrusion into oil, degasification, regain of gas in oil, and the recent large salt fall in Cavern 103 (Figure 1). This latter event and the detailed follow-up analyses presented the SPR project with observations of caverns during their development which had never been previously realized (Ehgartner and Sobolik, 2002).

Within the SPR complex, deformation models of salt behavior have been used (Munson, 1998 and 1999). Generally, we have treated salt within a dome as an isotropic homogeneous medium in terms of its mechanical and dissolution behavior. Recent work (Munson *et al.*, 2003) specific to the Big Hill site implies that this assumption may not have been correct.

A previous report (Ehgartner *et al.*, 2002) examined several creep tests on Big Hill salt and concluded that the salt is weak in comparison to other salts. The creep tests were performed at different stress levels for use in deriving creep parameters. The stress levels chosen for the tests were expected to be well below the damage level for typical salt. However, the strain rates taken from the creep tests suggest that in each case, the salt was damaged. This invalidates the use of the test results for defining creep parameters and for subsequent creep analyses simulating cavern deformation, but demonstrates the salt damages much easier in comparison to published results for other salts, including salt tested from other SPR sites. Different failure criteria for Big Hill salt are plotted in Figure 2 in terms of the stress invariants (Ehgartner and Lee, 2003).

Since the creep tests were limited to only four stress levels and damage was noted in all cases, the data do not define the minimum strength of the salt. Stress levels below those tested during the creep experiments may also damage the salt. A criterion may be proposed for the maximum strength of the salt, but it must be recognized that it is not conservative. Figure 2 shows the maximum strength criteria based on the creep test results. For comparison, the criterion describing the typical strength of salt is also shown. At best, based on the creep tests, the strength of Big Hill salt is less than 60 percent that of typical salt.

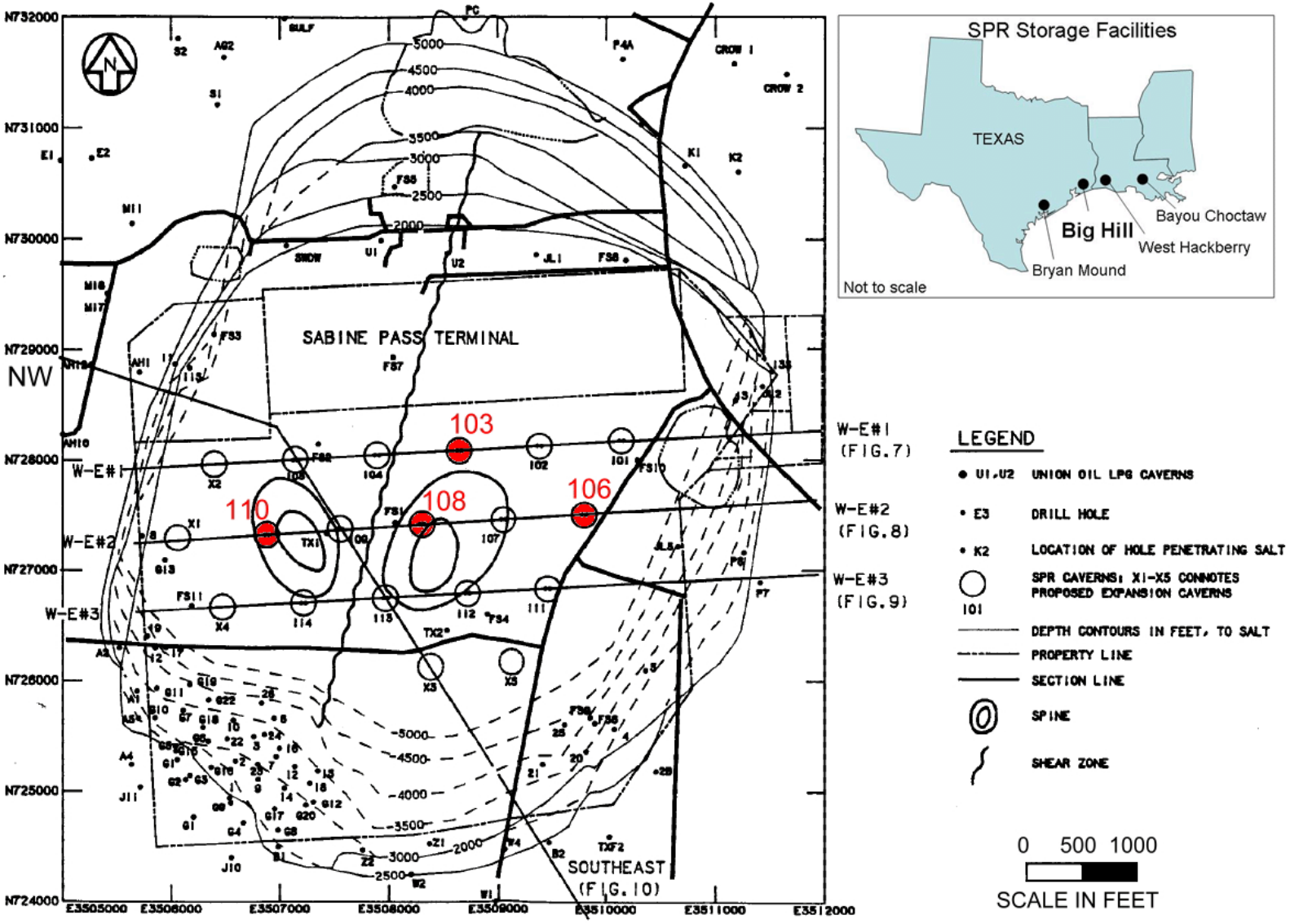

Figure 1. Big Hill salt dome structure map and location of caverns (modified after Magorian and Neal, 1988).

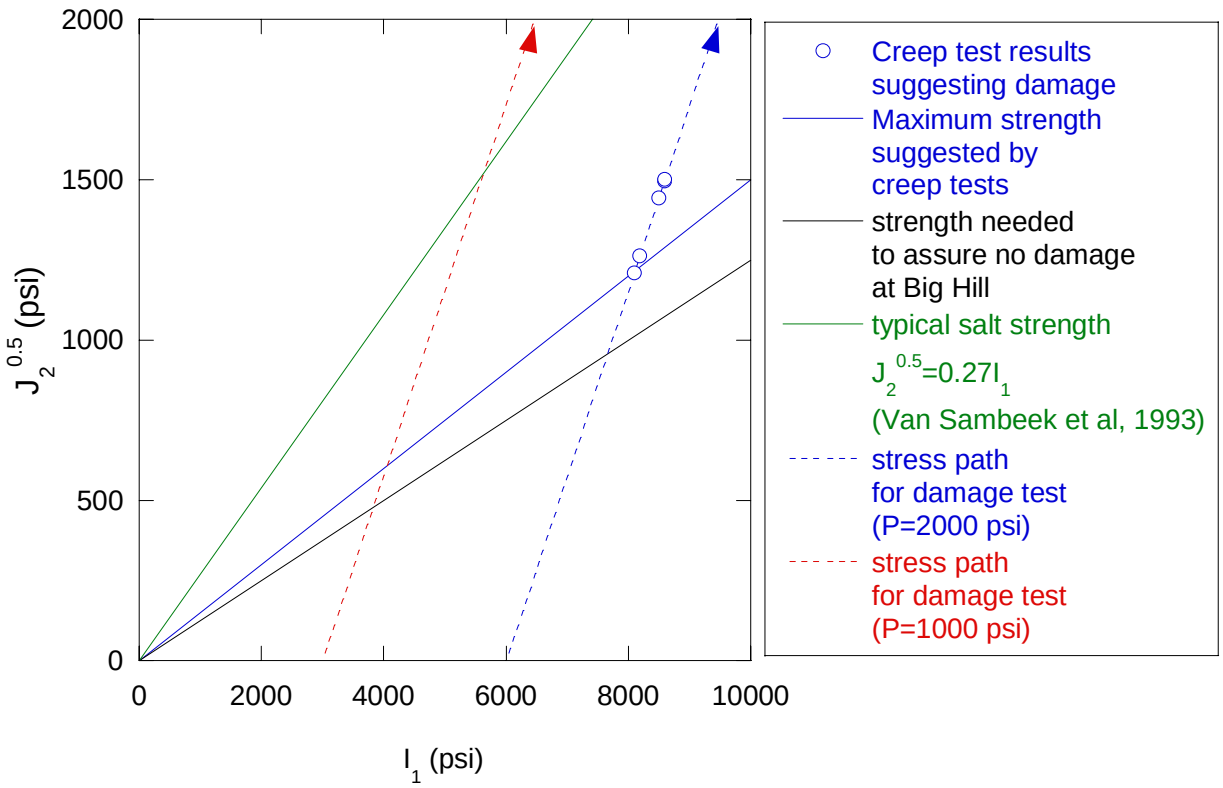

Figure 2. Creep test results and damage criteria (Ehgartner and Lee, 2003).

This maximum strength criterion was applied to the recently published 3-D cavern analyses (Ehgartner and Sobolik, 2002). The drops in safety factor in the plot represent work-over modes occurring at different places in the cavern field. The current age of Big Hill caverns is approximately 16 to 21 years since leaching. The 3-D analyses showed that during that time period, the factor of safety against damage dropped to approximately 1.2 using the maximum strength criteria, when the cavern was in the work-over mode. Figure 3 shows the results of the stress analyses after post-processing with the maximum strength criterion for Big Hill salt. The low strength of Big Hill salt does not present a problem during normal operational pressures, but safety factors approaching one are predicted using this model during times of workover. Figure 2 provides the strength criteria that would result in a safety factor of one, and hence damage of Big Hill salt. The strength of Big Hill salt must exceed the criteria (red line on plot) in order to assure no damage occurs in the analyses.

The safety factor predicted in the analyses is based on a non-conservative strength estimate which is greater than actually existing at Big Hill. This means the 3-D model (Ehgartner and Sobolik, 2002) results are not conservative and that the salt at Big Hill may have been damaged during times of low operating pressure. As damage and attendant cracking accumulate in the cavern walls, gas release and flow are facilitated. The damaged salt with diminished strength is left more susceptible to further deformation even when the cavern is repressurized, possibly resulting in salt falls.

To define the dilatant damage criteria for Big Hill salt, one uniaxial compression test and nine tiaxial compression tests have been completed under the quasi-static loading condition. The results are summarized in Table 1. The damage criteria established from these triaxial tests for Big Hill Salt will be implemented in the 3-D model analyses to determine if damage is predicted at low operating pressures. The relationship between dilatant damage and permeability can then be used to predict gas inflow into caverns.

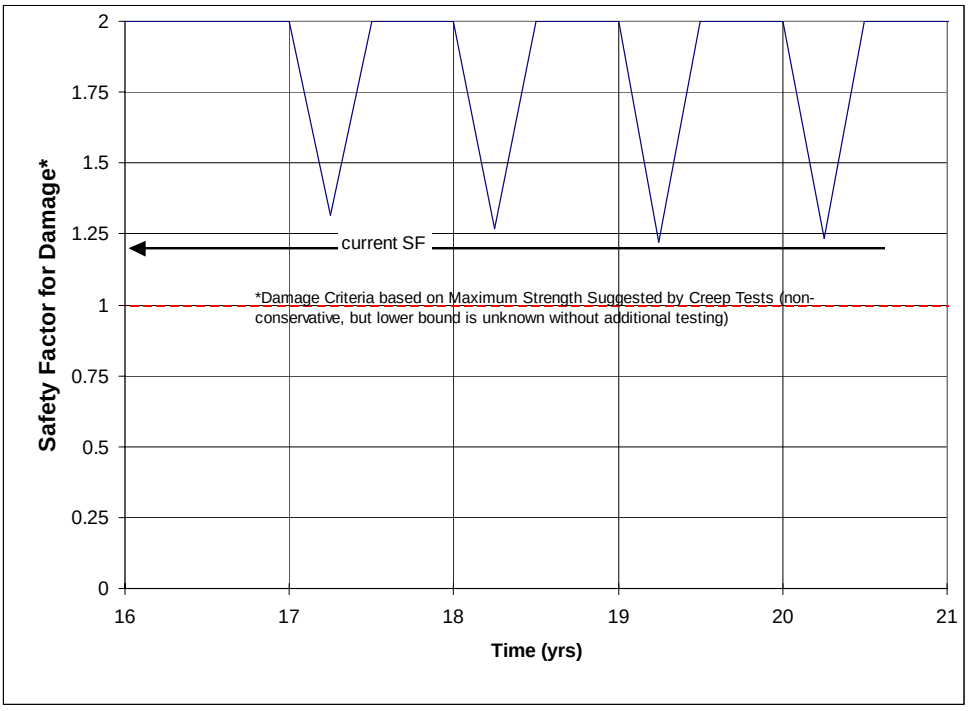

Figure 3. 3-D Analysis results using maximum Big Hill salt strength (Ehgartner and Sobolik, 2002).

Table 1. Triaxial compression test-matrix for Big Hill salt.

Test I.D.	Well I.D.	Depth (ft) (ft)	Confining Pressure, P (psi)
BHS-UC01	108B	4516	0
BHS-TA01	103B	4645 to 4650	1000
BHS-TA02	103B	4645 to 4650	2000
BHS-TA03	103B	4645 to 4650	1000
BHS-TA04	110B	4520	2000
BHS-TA05	106B	5465	1000
BHS-TA06	106A	2520	2000
BHS-TA07	108B	4516	1000
BHS-TA08	108B	4520	2000

2. Sample Preparation and Test Set-up

Because of the limited core inventory available for laboratory testing, several pieces of 4 inch diameter core were fabricated into smaller specimens. Table 2 shows the core inventory for Big Hill salt.

Table 2. Available 4" diameter core inventory for Big Hill salt.

Well	Depth (ft)	Length (inch)
103 B	4645 to 4650	10
103 B	4645 to 4650	6.5
103 B	4645 to 4650	10.5
103 B	4645 to 4650	9.5
103 B	4645 to 4650	4.5
103 B	4645 to 4650	5
106 A	2520	17.5
106 B	5465	17.5
108 B	4516	12
108 B	4520	11.5
110 B	4520	21

For triaxial compression testing, the Big Hill salt core was prepared in the form of a right circular cylinder (Figure 4) with nominal dimensions of 1.75 inch in diameter and 3.5 inch in length. The dimensions fell within the range of length-to-diameter ratio (2 to 2.5) recommended in ASTM D4543 ("Standard Practice for Preparing Rock Core Specimens and Determining Dimensional and Shape Tolerances"). The ends of the specimen were ground flat within 0.001 inch tolerance. Each specimen was visually inspected for significant flaws and general straightness of circumferential surfaces. The machined specimen was placed between cylindrical end-caps of the same diameter (Figure 4). The specimen assembly was coated with an approximately 0.05 inch thick impervious polyurethane membrane (Figure 4). To maintain uniform thickness of the membrane during curing, the specimen assembly was turned on a lathe along the axial centerline of the assembly. The polyurethane membrane allows the confining pressure to be applied hydrostatically on the specimen and at the same time prevents the confining fluid from infiltrating into the specimen. Two axial LVDT's (Linear Variable Displacement Transducers) and a Schuler gage (Schuler, 1978) were mounted on the specimen to measure axial and the lateral displacements, respectively (Figure 5). The instrumented specimen assembly was placed in a triaxial pressure vessel. The vessel is equipped with feed-throughs (Figure 5) for transmitting data from the LVDT's and the internal load-cell to the external data acquisition system.

Figure 6 shows the axial stress (σ_a)-time and pressure (P)-time history plots of a triaxial compression test. The first 16.5 hours of the record show a damage healing process adopted to heal the cracks in the salt core exposed without confining in situ stresses for an extended period of time. Stormont (1990) had reported the reduction of the permeability of WIPP salt that was

initially damaged and then subjected to healing under hydrostatic pressure. Figure 7 shows an example of the effect of damage healing process to the permeability of the salt. The healing process for Big Hill salt consisted of the placing the coated specimen under 4,000 psi confining pressure for about sixteen hours allowing open cracks to close and heal.

Figure 4. Big Hill salt specimens (left-before testing without coating; right-after testing with polyurethane coating).

Figure 5. Instrumented Big Hill salt specimen exposed after triaxial compression testing. Shown are two axial LVDT's and a Schuler gage mounted on the specimen to measure axial and the lateral displacements, respectively.

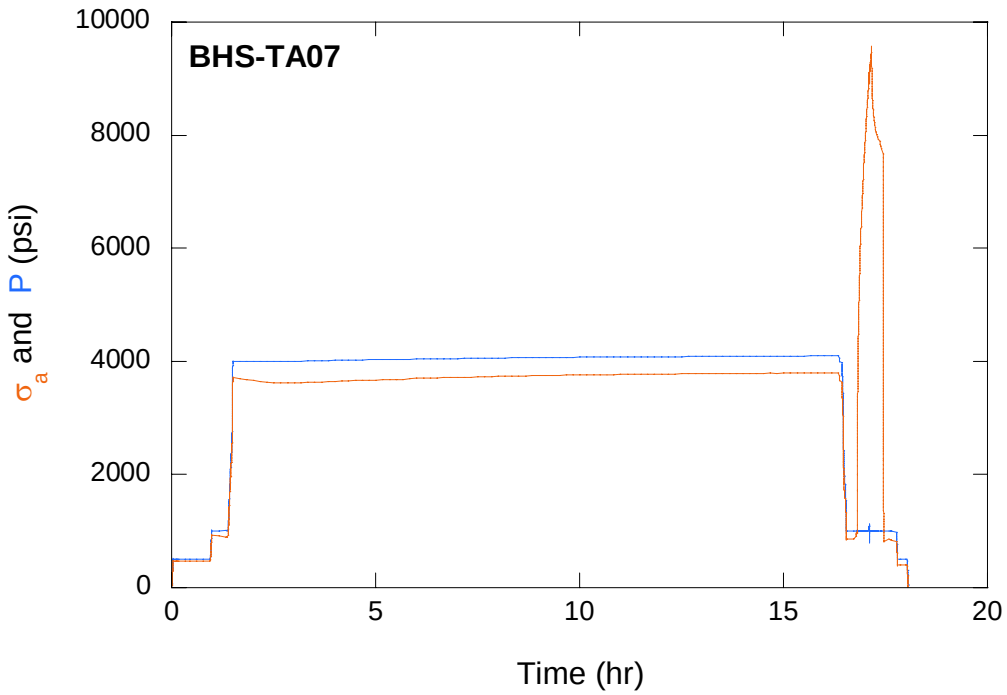

Figure 6. Axial stress (σ_a)-time and pressure (P)-time history plots of a triaxial compression test consisting of about 16.5 hours of healing cracks at 4,000 psi pressure followed by triaxial compression testing at 1,000 psi confining pressure.

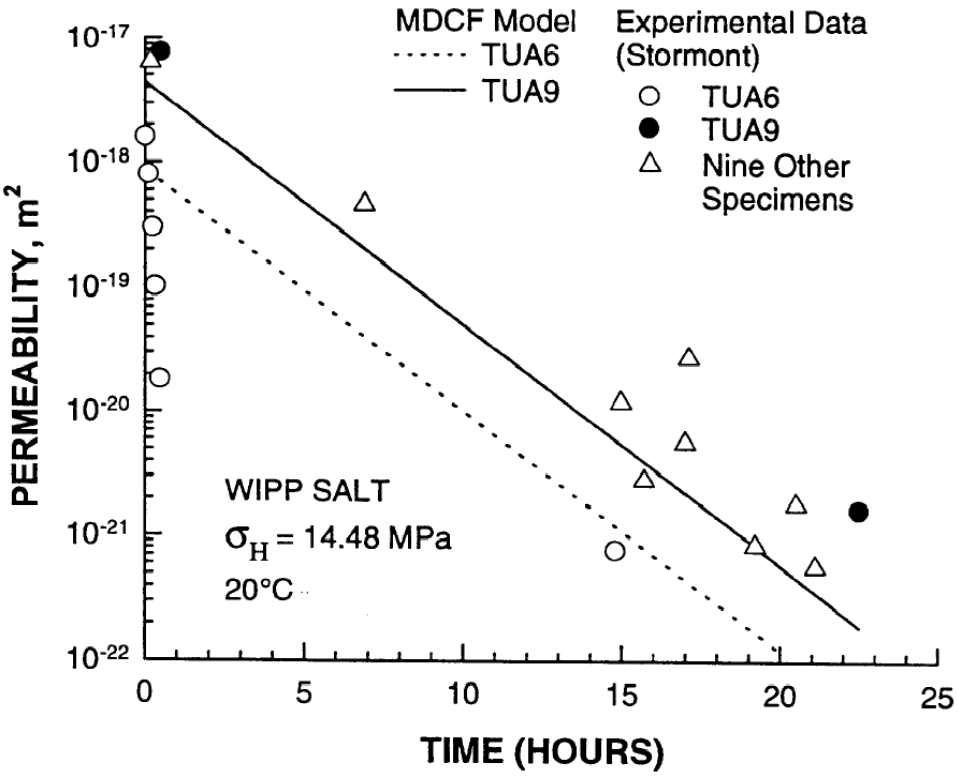

Figure 7. Effect of damage healing process on permeability of WIPP salt (Stormont, 1990).

3. Triaxial Compression Test of Big Hill Salt

After approximately sixteen hours of damage healing process of Big Hill specimen, the confining pressure was lowered to a level predetermined for a triaxial compression test. The specimen was loaded axially at a constant axial strain rate of 10^{-4} /s. The specimen was loaded until about 10% of axial strain was reached. An example of the strain vs. axial stress plot, recorded during a triaxial test of BHS-TA08, is shown in Figure 8. The axial stress, σ_a, is plotted against axial strain, ε_a, and lateral strain, ε_l (Figure 8). The volumetric strain, calculated as ($\varepsilon_v = \varepsilon_a + 2\varepsilon_l$), is also shown in the same plot.

To define the damage criteria for Big Hill salt, eight quasi-static triaxial compression tests and a uniaxial compression test have been carried out. The axial stress for the dilation limit ($\sigma_{a,d}$) in which the volume of the specimen reaches the minimum point, was used as the stress level required for dilatant damage to Big Hill salt. The damage stress of Big Hill salt was calculated from the following equation:

$$\sigma_{a,d} = P_{a,d} / \pi r^2$$

where $\sigma_{a,d}$ is the dilatant damage stress of salt in psi; $P_{a,d}$ is the load for $\sigma_{a,d}$ in lbs determined at the dilation limit; and r is the radius of the specimen in inches. The results are summarized in Table 3 and test records are shown in Appendices A, B, and C.

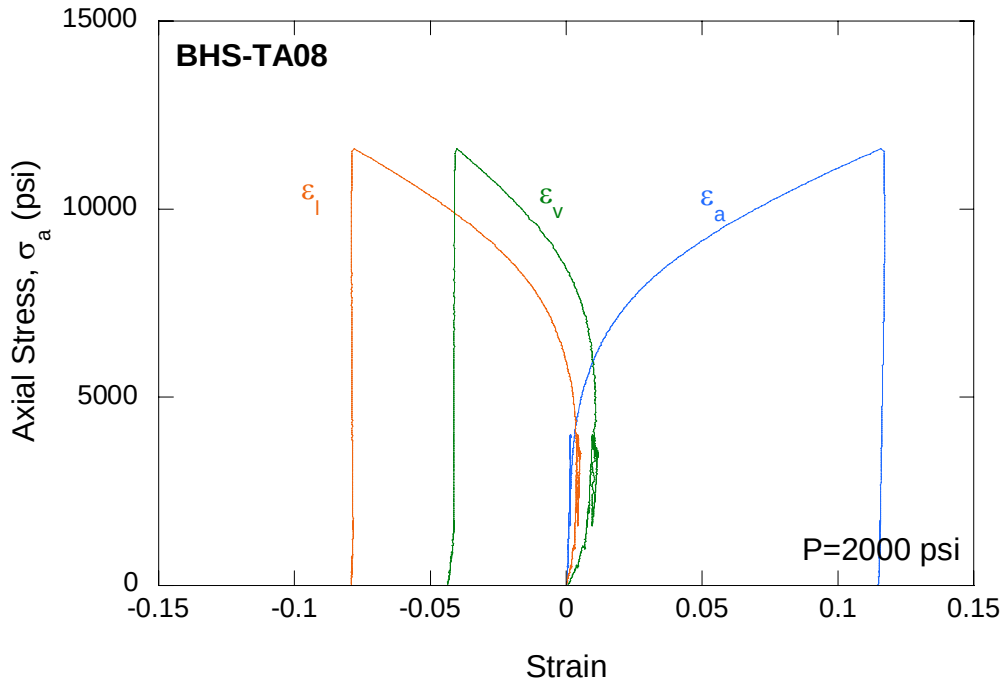

Figure 8. The stress-strain plot obtained from test BHS-TA08 consisting of hydrostatic compression up to 2,000 psi of confining pressure, P, followed by triaxial compression testing (σ_a - axial stress, ε_a - axial strain, ε_l - lateral strain, and ε_v - volumetric strain).

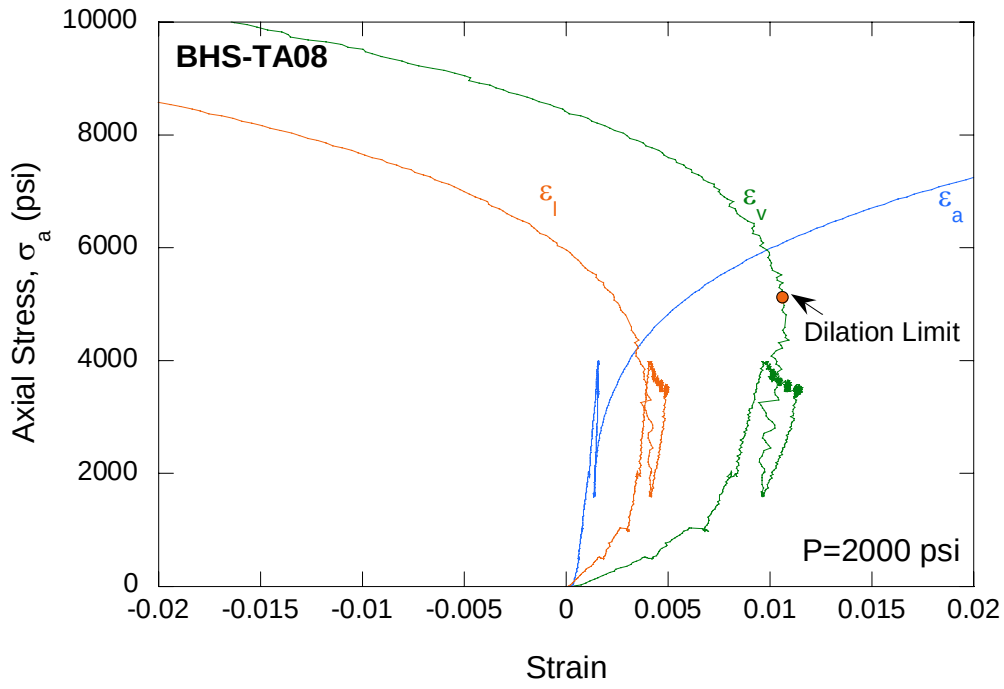

Figure 9. The enlarged stress-strain plot for test BHS-TA08. Dilation limit is indicated as the state of stress corresponding to the minimum volume of the specimen.

4. Dilatant Damage Criteria for Big Hill Salt

When rock salt is loaded, it initially compresses elastically (plastic strains do not affect the volume of the rock). As stress difference (σ_1- σ_3) is further incremented, micro-cracking becomes prominent and the volumetric strain deviates from the elastic deformation. In fact, the volume of the salt will increase due to the generation of additional pore space through micro-cracking. As damage accumulates, the permeability also increases and at some point the specimen reaches its ultimate strength and fails.

The onset of dilatant damage can be defined in several ways. However, for consistency with the literature (Mellegard and Pfeifle, 1994), it will be defined as the point at which the rock reaches its minimum volume (or dilation limit). Dilatancy criteria typically relate two stress invariants: the mean stress invariant I_1 and the square root of the invariant stress deviator J_2. Table 3 summarizes the results from our laboratory experimental program of Big Hill salt consisting of eight triaxial compression tests and a uniaxial compression test. The cap plasticity model (Sandler and Rubin, 1979) is formulated in terms of two stress invariants. In the triaxial compression tests, the axial stress was the major principal stress, σ_1, and the confining pressure, P, was acting as the intermediate, σ_2, and the minimum, σ_3, principal stresses, respectively. Then, the stress invariants at the onset of dilation can be described as,

$$I_1 = \sigma_1 + \sigma_2 + \sigma_3 = \sigma_{a,d} + 2P$$

$$\sqrt{J_2} = \sqrt{\frac{(\sigma_1 - \sigma_2)^2 + (\sigma_2 - \sigma_3)^2 + (\sigma_3 - \sigma_1)^2}{6}} = \frac{(\sigma_{a,d} - P)}{\sqrt{3}}$$

The critical values of I_1 and $\sqrt{J_2}$ for different confining pressures are listed in Table 3. During the dilatant damage of the specimens, the state of stress can be represented by the following exponential equation (Sandler and Rubin, 1979 and Fossum *et al.*, 1995).

$$\sqrt{J_2} = A - B\exp^{CI_1}$$

where A, B, and C are unknown parameters to be determined for Big Hill salt.

We used a nonlinear regression analysis to determine the unknown parameters A, B, and C, which minimized the sum of the squares of errors between the model-predicted values of $\sqrt{J_2}$ and the observed values of $\sqrt{J_2}$ for different values of I_1. For Big Hill salt, the dilatant damage envelopes are best represented by the following equation (Figure 10):

$$\sqrt{J_2}\,(psi) = 1746 - 1320.5\exp^{-0.00034 I_1\,(psi)}$$

The same damage data from the triaxial compression tests may also be described in terms of the principal stresses.

$$\sigma_{a,\,d} = C_{a,\,d,\,p} + q\sigma_3$$

where $\sigma_{a,\,d}$ is the predicted major principal stress (σ_1) at the dilation limit; $C_{a,\,d,\,p}$ is the predicted value of uniaxial damage strength ($C_{a,\,d}$) determined from the dilation limit; σ_3 is the minor principal stress generated by the confining pressure; and q is the slope of the best-fit straight line.

For Big Hill salt, the dilatant damage envelope is best represented by the following linear equation:

$$\sigma_{a,\,d}\,(psi) = 2248 + 1.25\ \sigma_3\,(psi)$$

The slope of the best-fit linear line for Big Hill salt can be related to the coefficient of internal friction ϕ as follows.

$$q = [\sqrt{(\phi^2 + 1)} + \phi]^2$$

Thus, the coefficient of internal friction for Big Hill salt is approximately 0.11.

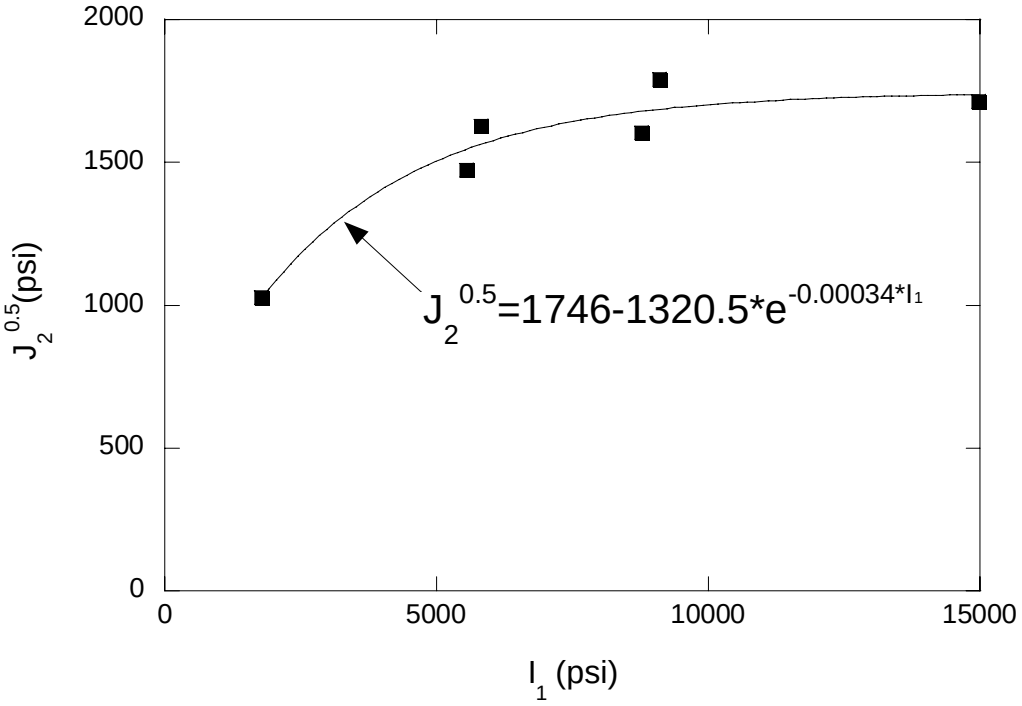

Figure 10. Dilatant damage criterion of Big Hill salt represented by the stress invariants $I_1=\sigma_1+\sigma_2+\sigma_3$ and $J_2 = [(\sigma_1-\sigma_2)^2 + (\sigma_2-\sigma_3)^2 + (\sigma_3-\sigma_1)^2]/6$.

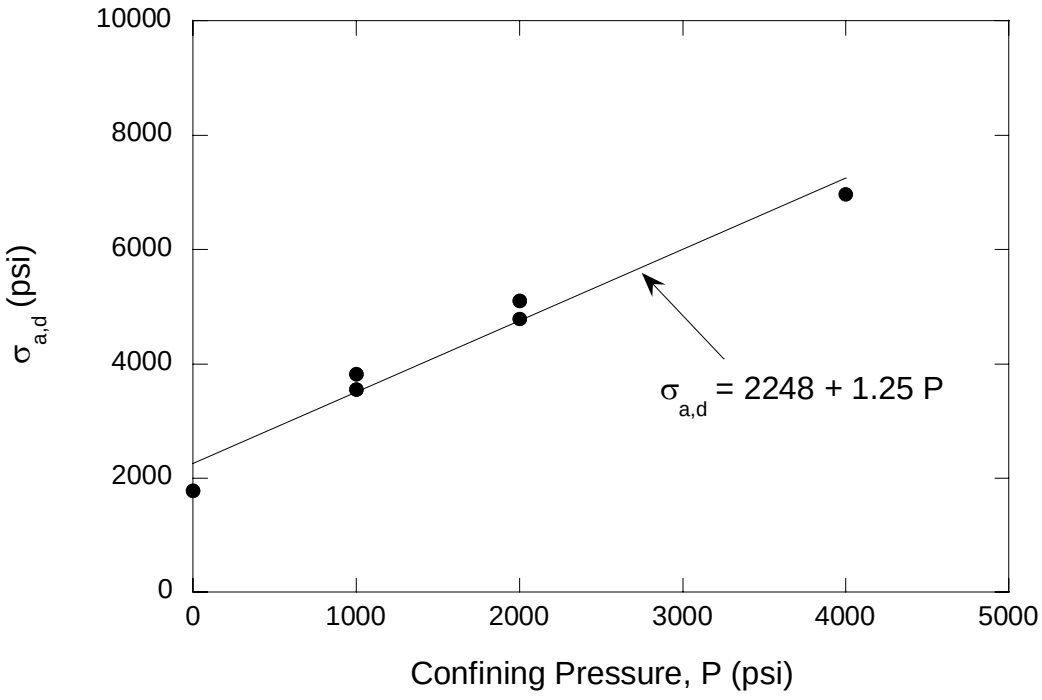

Figure 11. Dilatant damage criterion of Big Hill salt represented in terms of principal stresses; axial stress for the dilation limit ($\sigma_{a,d}$) and the confining pressure (σ_3 =P).

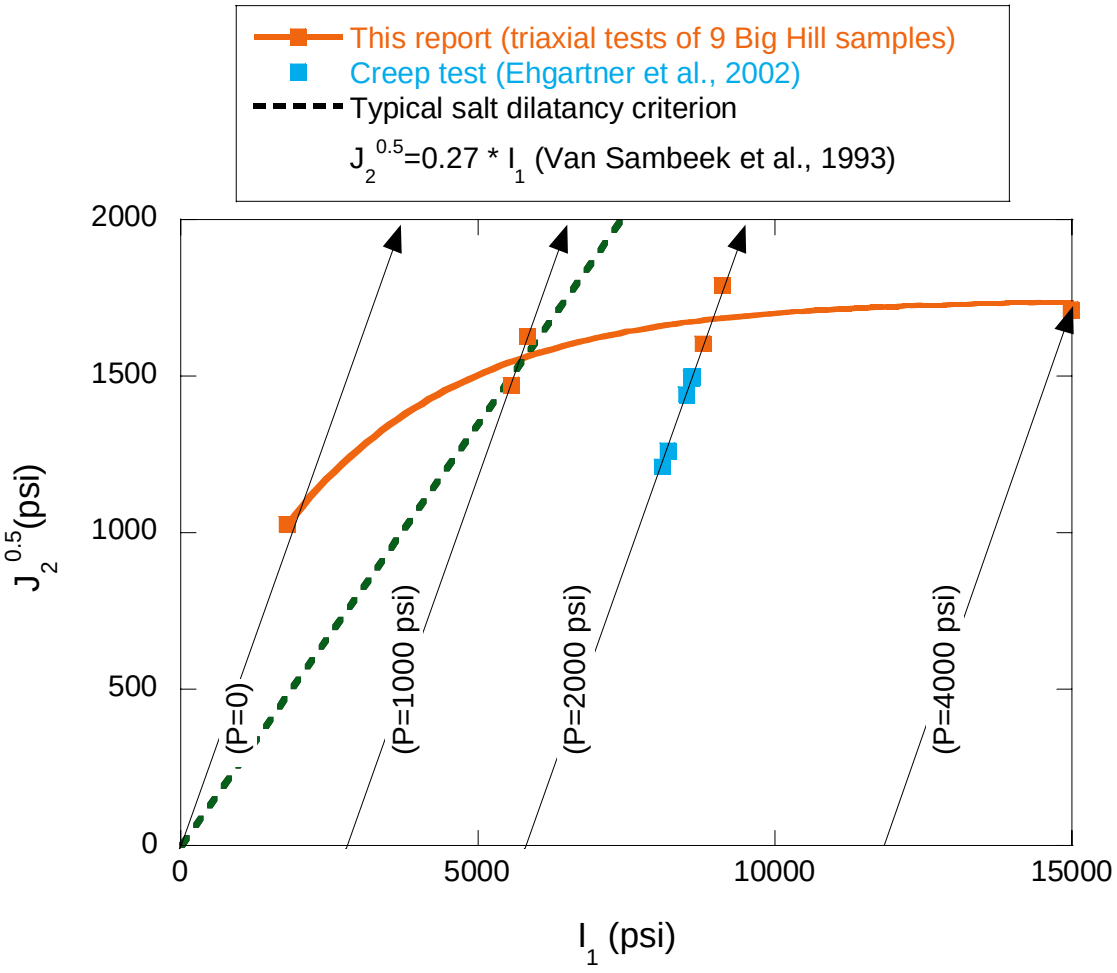

Figure 12. Dilatant damage criterion of Big Hill salt compared to the damage stress suggested by the creep tests.

Our concern, based on the recent massive salt fall (Munson *et al.,* 2003) and gas regain rates in certain Big Hill caverns, is that we have underestimated the strength values used in past analyses. A previous report (Ehgartner *et al.,* 2002) examines several creep tests on Big Hill salt and concludes that the salt is weak in comparison to other salts. The average volume content of the insoluble impurities for the SPR domal salts for Big Hill is 4.97% compared to 3.94% for West Hackberry, 1.74% for Bayou Choctaw, and 4.13% for Bryan Mound (Munson, 2000). The effect of clay contents on lowering shear damage in salt has been formulated by Chan *et al*. (2000) for argillaceous salt. However, for Tioga salt (Ehgartner, 1996 and Lee and Ehgartner, 2001), the dilatancy boundary obtained from triaxial testing shows an increase in terms of $\sqrt{J_2}$ as the impurity content is increased. It is unclear how the contents of impurities such as polyhalite, anhydrite, clay, and silicate particles existing in Big Hill salt can be attributed to the level of dilatancy boundary.

The creep tests were performed at different stress levels for use in deriving creep parameters. Figure 12 shows the comparison of different damage strength criteria. The results from our laboratory experiments of Big Hill salt show that the general trend of the dilatant damage criteria is nonlinear in terms of stress invariants. For the confining pressure of 1,000 psi, the typical salt strength represented as $\sqrt{J_2}$ =0.27 I_1 (Van Sambeek *et al*., 1993) is virtually equal to the dilatant damage strength of Big Hill salt determined by this experimental program. However, for higher confining pressure, the typical strength criterion overestimates the damage strength of Big Hill salt. Figure 12 also shows the maximum strength criteria based on the creep test slightly underestimate the damage strength of Big Hill salt. We are uncertain that stress levels below those tested during the creep experiments may damage the salt. We are also uncertain that the strain rate differences used for testing may result in the differences in damage strengths. In order to validate the relationship between the damage strength criteria, it is recommended that creep tests at 1,000 psi confining pressure be conducted.

Table 3. Summary of uniaxial / triaxial compression tests of Big Hill salt.

Specimen no.	Well no.	Depth (ft)	Diameter (inch)	Length (inch)	Weight (g)	Density (pcf)	P (psi)	$\sigma_{a,\,d}$ (psi)	I_1 (psi)	$\sqrt{J_2}$ (psi)
BHS-UC01*	108B	4516	1.747	3.692	323.00	139.0	0	1780	1780	1028
BHS-TA01	103B	4645	1.750	3.520	308.20	138.8	1000	3820	5820	1628
BHS-TA02	103B	4645	1.749	3.564	309.60	137.7	2000	4780	8780	1605
BHS-TA03	103B	4645	1.750	3.530	310.27	139.2	1000	3550	5550	1472
BHS-TA04	103B	4520	1.748	3.501	322.27	146.2	2000			
BHS-TA05	110B	5468	1.749	3.400	308.80	144.0	4000	6970	14970	1715
BHS-TA05	106B	2520	1.749	3.438	NA	NA	1000			
BHS-TA06	106A	2520	1.749	3.461	299.85	137.5	2000			
BHS-TA07	108B	4516	1.749	3.484	301.06	137.1	1000			
BHS-TA08	108B	4520	1.747	3.692	323.00	139.0	2000	5100	9100	1790

*-unconfined uniaxial compression test

$\sigma_{a,\,d}$-dilatant damage stress obtained from the dilation limit

P-confining pressure

$I_1=\sigma_{a,\,d}+2P$

$\sqrt{J_2} = (\sigma_{a,\,d}-P)/\sqrt{3}$

5. Permeability Measurements of Big Hill Salt in Relation to Dilatation

The dilatant damage criteria and coupled permeability could be used in modeling the performance of the caverns, examining stability and gas intrusion consequences at low operating pressures, and defining acceptable operating levels. This will provide information relating the state of stress causing dilatant damage to the permeability used for assessing gas intrusion into caverns operated at different pressures. The coupling between damage and permeability is important since even minor amounts of dilatant damage can result in large changes in the permeability of salt. For example, Peach (1991) has shown the permeability of Asse salt to increase five orders of magnitude over its undamaged value (10^{-9} Darcy) during dilatant damage resulting in a one percent increase in volume. The damage-induced permeability may be an important factor in understanding and controlling gas intrusion.

The gas permeability of Big Hill salt was measured in conjunction with a triaxial compression test using a constant-head permeameter set-up (Figure 13) which duplicates Darcy's classic experiment with constant pressure differential and steady state of flow through a specimen. Helium gas was used as a flowing medium. The end-caps used in triaxial compression tests had a flow port to allow Helium to go through the specimen. Permeable disks, made out of a felt material, coupled the end-caps to the specimen. The confining pressure was controlled to be constant by a servo-control system. The pressure differential in Helium gas was controlled by a gas regulator. The gas permeability of the specimen, k, is calculated by the following Darcy's equation:

$$k_{He} = Q_x \cdot \mu \cdot L / (A \cdot \Delta P)$$

where k_{He} is the Helium gas permeability (Darcy)
Q_x is the flowrate in the axial direction of the specimen (cm^3/s)
μ is the viscosity of Helium
ΔP is the pressure differential measured across the ends of the specimen (atm)
L is the length of the specimen (cm), and
A is the cross-sectional area perpendicular to the axis of the specimen (cm^2).

The permeability of Big Hill salt was measured at different stages of healing and dilatant damage processes in the specimen. Table 4 summarizes the resulting permeability measurements. Before the healing process was instigated, permeability measurements were conducted at different confining pressures. The reduction in permeability is obvious as the confining pressure is increased for each specimen. The permeability reduction in Big Hill salt is probably controlled by reduction in apertures of existing cracks of the salt by increasing the mean stress on the specimen. The healing process reduced the permeability but the resulting permeability was on the same order as the initial one. The unexpected result was the permeability values obtained after the specimen went through dilatant damage processes. The salt specimen remained in the triaxial pressure vessel during the permeability testing as the mechanical and hydrologic test procedures are integrated into the same test machine (Figure 13). The increase in permeability in

relation to dilatant damage was not clear in all Big Hill salt specimens we tested. In some cases (BHS-TA02 and BHS-TA03), permeability appears to be reduced during and after the dilatant failure of the specimen. One possible cause of this unexpected result may be stemming from the ends of the specimen contacting the end-caps through the permeable disk. The dilatant damage to the specimen was observed from the test record (Appendix C) and also from the specimens (Figures 4 and 5) removed from the pressure vessel after the test. A typical shape of the failed specimen was a barrel shape indicating inhomogeneous damage to the specimen. As shown in Figure 14, the end of the specimen contacting the end-cap through the permeable disk was not deformed due to friction between the specimen and the permeable disk. The undeformed ends of the specimen showed no communication with dilatant damage zones located in the middle of the specimen. To measure permeability in the dilatant damage zone of the specimen, the ends of the specimen were trimmed about ¼" in length. Figure 14 shows the exposed fractures after the ends of the specimen were trimmed. The end-ground specimen showed increase in permeability in all cases. In BHS-TA04, 05, 06, and 07 specimens, an increase in permeability coupled with dilatant damage was observed. However, in BHS-TA02, 03, and 08 specimens, post-damage measurements did not indicate increases in permeability.

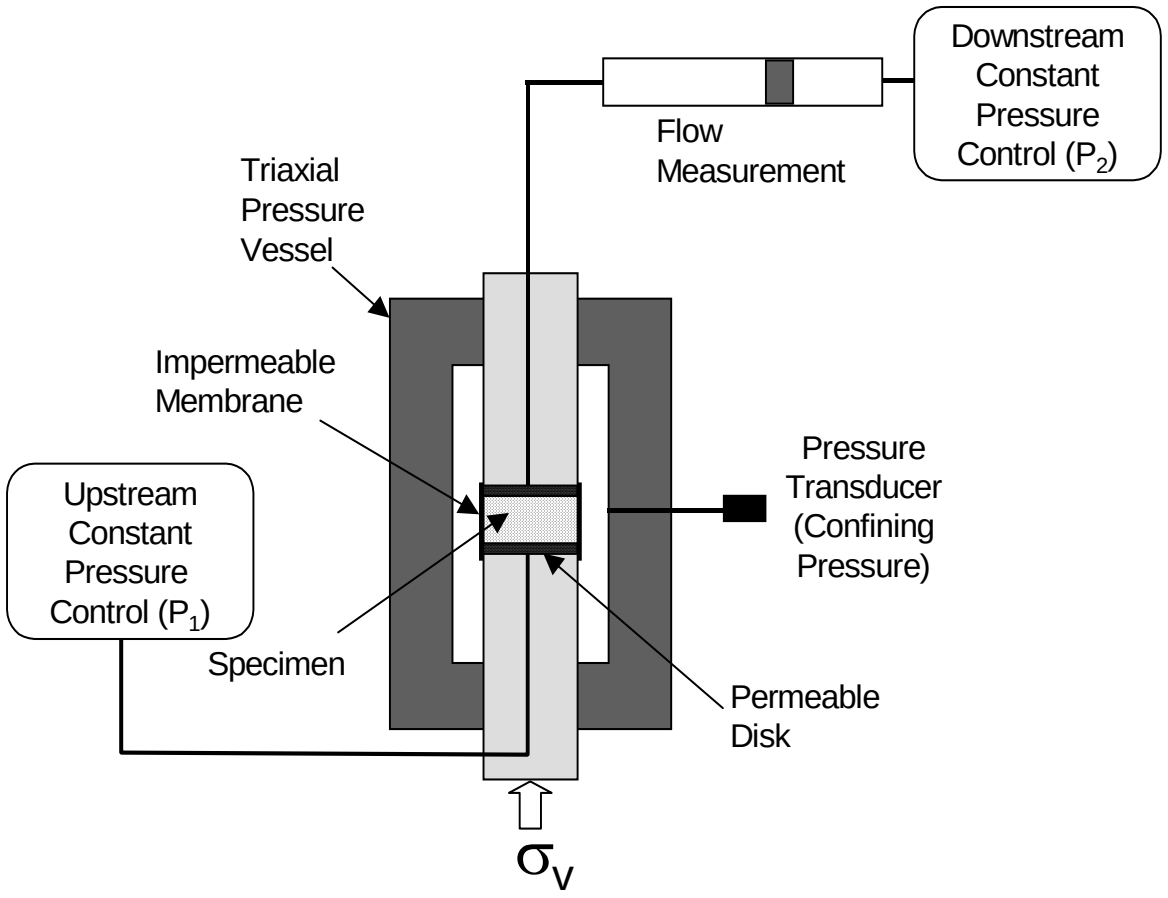

Figure 13. Constant-head gas permeability measurement set-up used for Big Hill salt in conjunction with triaxial compression testing.

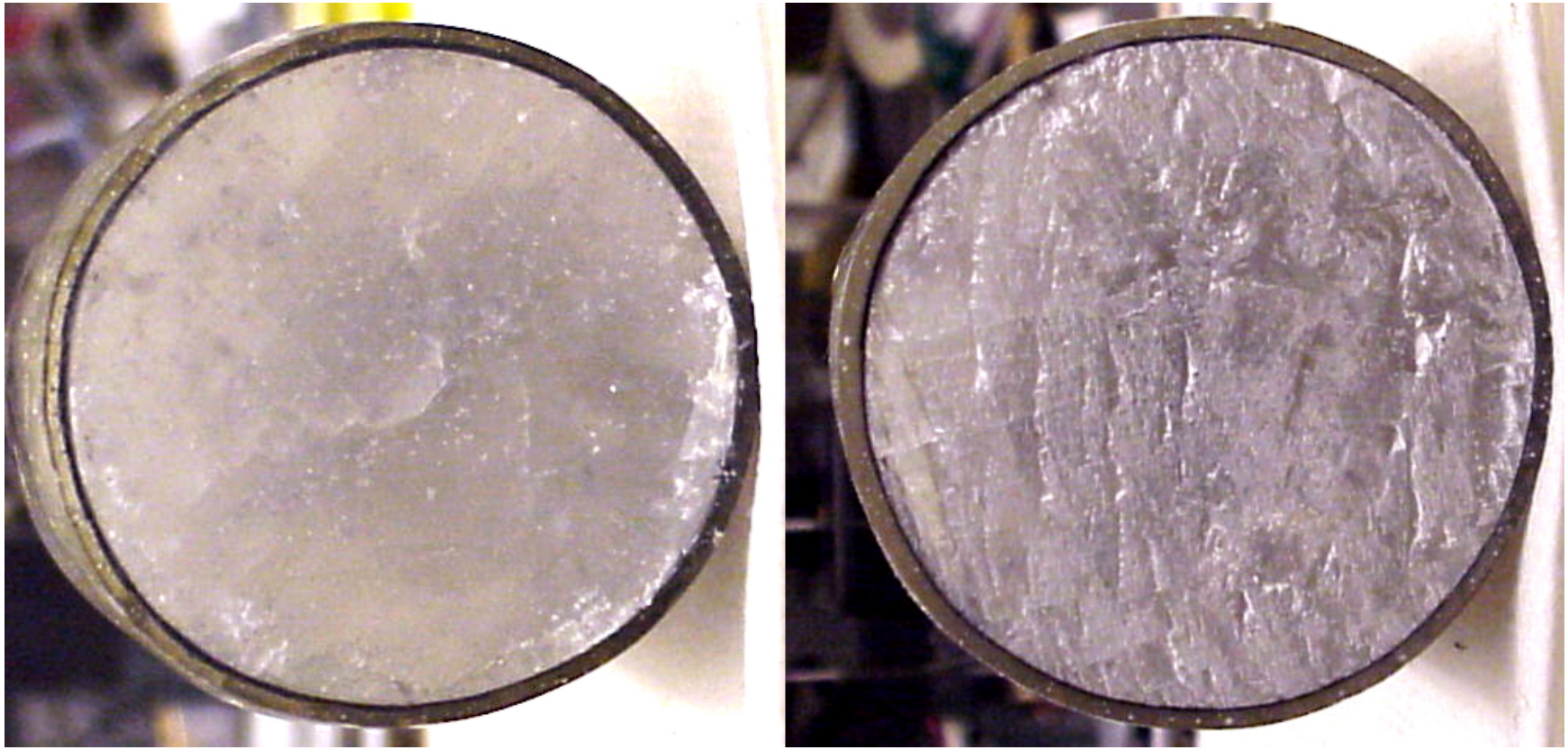

Figure 14. BHS-TA06 specimen after triaxial compression testing. The undeformed end surface contacting the end-cap is shown in the left picture. The trimmed end surface of the same specimen reveals extensive fracturing.

Table 4. Summary of gas (Helium) permeability measurements of Big Hill salt.

Sample I.D	Test condition	Pressure P (psi)	Diameter (cm)	Length (cm)	Cross-sectional area, A (cm^2)	He pressure ΔP (atm)	Q_x (cm^3/s)	Permeability k_{He} (10^{-6} Darcy)
BHS-TA01	Initial	1000	4.444	8.997	15.509	0.68	6.0E-03	100
BHS-TA01	Initial	2000	4.444	8.997	15.509	0.68	4.3E-03	72
BHS-TA01	Initial	3000	4.444	8.997	15.509	0.68	3.7E-03	61
BHS-TA01	Healed	3000	4.444	8.997	15.509	0.68	5.2E-03	86
BHS-TA02	Initial	1000	4.547	9.053	16.235	0.68	2.2E-01	3478
BHS-TA02	Initial	2000	4.547	9.053	16.235	0.68	1.6E-01	2595
BHS-TA02	Initial	3000	4.547	9.053	16.235	0.68	1.0E-01	1659
BHS-TA02	Initial	4000	4.547	9.053	16.235	0.68	8.0E-02	1284
BHS-TA02	Healed	4000	4.547	9.053	16.235	0.68	4.8E-02	776
BHS-TA02	Healed	2000	4.547	9.053	16.235	0.68	1.2E-01	1900
BHS-TA02	During TC	2000	4.547	9.053	16.235	0.68	8.3E-03	134
BHS-TA02	Post TC	2000	4.547	9.053	16.235	0.68	8.3E-03	134
BHS-TA02	Post TC	1000	4.547	9.053	16.235	0.68	1.0E-02	161
BHS-TA02	Post TC	500	4.547	9.053	16.235	0.68	1.3E-02	201
BHS-TA02	Post TC	200	4.547	9.053	16.235	0.68	1.5E-02	241
BHS-TA02	End ground	1000	4.547	8.001	16.235	0.68	3.0E-02	426
BHS-TA03	Initial	1000	4.445	8.966	15.518	0.68	3.0E-01	4991
BHS-TA03	Initial	2000	4.445	8.966	15.518	0.68	1.4E-01	2357
BHS-TA03	Initial	4000	4.445	8.966	15.518	0.68	9.2E-02	1525
BHS-TA03	Healed	4000	4.445	8.966	15.518	0.68	5.3E-02	887
BHS-TA03	During TC	2000	4.445	8.966	15.518	0.68	0.0E+00	0
BHS-TA03	Post TC	500	4.445	8.966	15.518	1.36	1.9E-01	1594
BHS-TA03	End ground	1000	4.445	7.391	15.518	0.68	2.3E-01	3086
BHS-TA03	End ground	2000	4.445	7.391	15.518	0.68	1.7E-01	2286
BHS-TA03	End ground	4000	4.445	7.391	15.518	0.68	1.3E-01	1749
BHS-TA04	Initial	1000	4.439	8.893	15.474	1.36	5.0E-04	4
BHS-TA04	Initial	1000	4.439	8.893	15.474	3.40	2.5E-02	83
BHS-TA04	Initial	2000	4.439	8.893	15.474	3.40	1.8E-02	61
BHS-TA04	Initial	4000	4.439	8.893	15.474	3.40	6.7E-03	22
BHS-TA04	Healed	4000	4.439	8.893	15.474	3.40	4.2E-03	14
BHS-TA04	Healed	2000	4.439	8.893	15.474	3.40	7.5E-03	25
BHS-TA04	During TC	2000	4.439	8.893	15.474	0.68	3.2E-02	524
BHS-TA04	Post TC	2000	4.439	8.893	15.474	0.68	3.3E-02	538
BHS-TA04	Post TC	1000	4.439	8.893	15.474	0.68	3.5E-02	579
BHS-TA04	Post TC	500	4.439	8.893	15.474	0.68	4.7E-02	772
BHS-TA04	End ground	500	4.439	7.493	15.474	0.68	1.5E-01	2091
BHS-TA04	End ground	1000	4.439	7.493	15.474	0.68	1.1E-01	1580
BHS-TA04	End ground	2000	4.439	7.493	15.474	0.68	8.7E-02	1208

Table 4. Summary of gas (Helium) permeability measurements of Big Hill salt (continued).

Sample I.D	Test condition	Pressure P (psi)	Diameter (cm)	Length (cm)	Cross-sectional area, A (cm^2)	He pressure ΔP (atm)	Q_x (cm^3/s)	Permeability k_{He} (10^{-6} Darcy)
BHS-TA05	Initial	2000	4.442	8.636	15.500	3.40	1.6E-02	51
BHS-TA05	Initial	4000	4.442	8.636	15.500	3.40	6.7E-03	21
BHS-TA05	During TC	4000	4.442	8.636	15.500	3.40	5.8E-03	19
BHS-TA05	Post TC	1000	4.442	8.636	15.500	3.40	1.4E-01	460
BHS-TA05	Post TC	1000	4.442	8.636	15.500	0.68	1.3E-02	214
BHS-TA05	Post TC	500	4.442	8.636	15.500	0.68	1.3E-02	214
BHS-TA05	End ground	1000	4.442	7.544	15.500	0.68	9.0E-02	1261
BHS-TA05	End ground	2000	4.442	7.544	15.500	0.68	5.5E-02	771
BHS-TA05	End ground	4000	4.442	7.544	15.500	0.68	2.5E-02	350
BHS-TA05	End ground	1000	4.442	7.544	15.500	0.68	4.0E-02	561
BHS-TA06	Initial	1000	4.442	8.733	15.500	0.68	0.0E+00	0
BHS-TA06	Initial	500	4.442	8.733	15.500	3.40	0.0E+00	0
BHS-TA06	Initial	1000	4.442	8.733	15.500	5.99	0.0E+00	0
BHS-TA06	During TC	2000	4.442	8.733	15.500	3.40	0.0E+00	0
BHS-TA06	Post TC	1000	4.442	8.733	15.500	3.40	0.0E+00	0
BHS-TA06	Post TC	500	4.442	8.733	15.500	3.40	1.3E-03	4
BHS-TA06	End ground	500	4.442	7.518	15.500	3.40	4.2E-02	116
BHS-TA06	End ground	1000	4.442	7.518	15.500	3.40	2.0E-02	56
BHS-TA06	End ground	2000	4.442	7.518	15.500	3.40	0.0E+00	0
BHS-TA07	Initial	500	4.441	8.791	15.491	0.68	0.0E+00	0
BHS-TA07	Initial	500	4.441	8.791	15.491	3.40	1.3E-02	41
BHS-TA07	Initial	1000	4.441	8.791	15.491	3.40	4.6E-03	15
BHS-TA07	During TC	1000	4.441	8.791	15.491	3.40	3.7E-02	120
BHS-TA07	Post TC	1000	4.441	8.791	15.491	3.40	5.0E-02	163
BHS-TA07	Post TC	1000	4.441	8.791	15.491	0.68	6.7E-03	109
BHS-TA07	Post TC	500	4.441	8.791	15.491	0.68	1.0E-02	163
BHS-TA07	End ground	1000	4.441	7.645	15.491	0.68	5.7E-02	805
BHS-TA07	End ground	4000	4.441	7.645	15.491	0.68	1.3E-02	189
BHS-TA07	End ground	1000	4.441	7.645	15.491	0.68	1.8E-02	261
BHS-TA08	Initial	500	4.441	8.849	15.491	0.68	2.0E-02	329
BHS-TA08	Initial	1000	4.441	8.849	15.491	0.68	7.5E-03	123
BHS-TA08	Initial	1000	4.441	8.849	15.491	3.40	6.0E-02	197
BHS-TA08	Initial	2000	4.441	8.849	15.491	3.40	1.3E-02	44
BHS-TA08	Initial	4000	4.441	8.849	15.491	3.40	5.0E-03	16
BHS-TA08	Healed	4000	4.441	8.849	15.491	3.40	3.3E-03	11
BHS-TA08	Healed	2000	4.441	8.849	15.491	3.40	4.2E-03	14
BHS-TA08	During TC	2000	4.441	8.849	15.491	3.40	4.2E-03	14
BHS-TA08	Post TC	2000	4.441	8.849	15.491	3.40	4.2E-03	14
BHS-TA08	Post TC	1000	4.441	8.849	15.491	3.40	5.0E-03	16
BHS-TA08	Post TC	500	4.441	8.849	15.491	3.40	2.0E-02	66
BHS-TA08	End ground	500	4.441	7.722	15.491	0.68	3.5E-02	502
BHS-TA08	End ground	1000	4.441	7.722	15.491	0.68	1.6E-02	227
BHS-TA08	End ground	2000	4.441	7.722	15.491	0.68	9.2E-03	132
BHS-TA08	End ground	2000	4.441	7.722	15.491	3.40	7.7E-02	220

6. Conclusions

To establish dilatant damage criteria of Big Hill salt, a series of quasi-static laboratory tests have been completed in conjunction with permeability measurements. The eight triaxial compression tests and a uniaxial compression test established dilatant damage criteria for Big Hill salt in terms of stress invariants (I_1 and J_2) and principal stresses ($\sigma_{a,\,d}$ and σ_3), respectively. The results can be summarized as follows:

- Under the triaxial compression stress condition ($\sigma_1>\sigma_2=\sigma_3=P$), Big Hill salt deforms elastically and then dilates due to accumulated damage incurred by micro-cracking.

- The dilatant damage criteria for Big Hill salt can be represented in terms of stress invariants and principal stresses, respectively:

$$\sqrt{J_2}\,(psi) = 1746 - 1320.5\exp^{-0.00034 I_1\,(psi)}$$

$$\sigma_{a,\,d}\,(psi) = 2248 + 1.25\;\sigma_3\,(psi)$$

- For the confining pressure of 1,000 psi, the dilatant damage strength of Big Hill salt is identical to the typical salt strength ($\sqrt{J_2} = 0.27\,I_1$). However, for higher confining pressure, the typical strength criterion overestimates the damage strength of Big Hill salt.

- The strength criteria based on the creep test slightly underestimates the damage strength determined by the triaxial tests of Big Hill salt.

- The coupling between dilatant damage and increase in permeability appears to exist in Big Hill salt.

References

ASTM D4543, Standard Practice for Preparing Rock Core Specimens and Determining Dimensional and Shape Tolerances, American Society for Testing and Materials, 1995.

Chan, K. S., Bodner, S. R. and D. E. Munson, Application of Isochronous Healing Curves in Predicting Damage Evolution in a Salt Structure, International Journal of Damage Mechanics, Vol. 9, pp. 131-153, April, 2000.

Ehgartner, B. L., Memo to Xavier Allemandou Market Hub Partners, August 16, 1996.

Ehgartner, B. L. and S. Sobolik, 3-D Cavern Enlargement Analyses, SAND2002-0526, Sandia National Laboratories, Albuquerque, New Mexico, March 2002.

Ehgartner, B. L., Bauer, S. J. and D. E. Munson, Big Hill Salt Strength, Draft Report to Robert E. Myers, DOE SPR PMO FE-4421, November 18, 2002.

Ehgartner, B. L. and M. Y. Lee, Memo to Robert E. Myers, DOE SPR PMO FE-4421, January 31, 2003.

Fossum, A. F., Senseny, P. E., Pfeifle, T. W. and K. D. Mellegard, Experimental Determination of Probability Distributions for Parameters of a Salem Limestone Cap Plasticity Model, Mechanics of Materials, Vol. 21, pp. 119-137, 1995.

Lee, M. Y. and B. L. Ehgartner, Laboratory Evaluation of Damage Criteria and Creep Parameters of Tioga Dolomite and Rock Salt from Cavern Well No. 1, SAND2001-0918, Sandia National Laboratories, Albuquerque, New Mexico, 2001.

Magorian, T. R. and J. T. Neal, Strategic Petroleum Reserve (SPR) Additional Geological Site Characterization Studies, Big Hill Salt Dome, Texas, SAND88-2267, Sandia National Laboratories, Albuquerque, New Mexico, 1988.

Mellegard, K. D. and T. W. Pfeifle, Laboratory Testing of Dome Salt from Weeks Island, Louisiana in Support of the Strategic Petroleum Reserve (SPR) Project, RSI-0552, RE/SPEC Inc, 1994.

Munson, D. E., Analysis of Multistage and Other Creep Data for Domal Salts, SAND98-2276, Sandia National Laboratories, Albuquerque, New Mexico, 1998.

Munson, D. E., Multimechanism-Deformation Parameters of Domal Salts Using Transient Creep Analysis, SAND99-2104, Sandia National Laboratories, Albuquerque, New Mexico, 1999.

Munson, D. E., Relative Evaluation of the Independent Volume Measures of Caverns, SAND2000-2041, Sandia National Laboratories, Albuquerque, New Mexico, 2000.

Munson, D. E., Bauer, S. J., Rautman, C., Ehgartner, B. L., and A. Sattler, Analysis of the Massive Salt Fall in Big Hill Cavern 103, SAND2003-0703, Sandia National Laboratories, Albuquerque, New Mexico, 2003.

Park, B. Y., Ehgartner, B. L., Lee, M. Y., and S. R. Sobolik, Defining the Allowable Standoff Distance for a Cavern to the Edge of the Dome Based on Big Hill Site, SAND Report, Sandia National Laboratories, Albuquerque, New Mexico, (in preparation).

Peach, C. J., Influence of Deformation on the Fluid Transport Properties of Salt Rocks, Geologica Ultraiectina, No. 77, April 10, 1991.

Sandler, I. S. and D. Rubin, An Algorithm and a Modular Subroutine for the Cap Model, Int. J. Numer. and Anal. Mech. Geomech., Vol. 3, pp.173-186, 1979.

Schuler, K. W., Lateral-Deformation Gage for Rock-Mechanics Testing, Experimental Mechanics, Vol. 18, No. 12, pp. 477-480, 1978.

Stormont, J. C., Gas Permeability Changes in Rock Salt During Deformation, Ph.D. Thesis, University of Arizona, Tucson, Arizona, 1990.

Van Sambeek, L. L, Ratigan, J. L., and F. D. Hansen, Dilatancy of Rock Salt in Laboratory Tests, Int. J. Rock Mech. Min. Sci. & Geomech. Abstr. Vol. 30, No. 7, pp. 735-738, 1993.

APPENDIX A

Time-Base Plots from Triaxial Compression Tests of Big Hill Salt

(σ_a-axial stress and P-confining pressure)

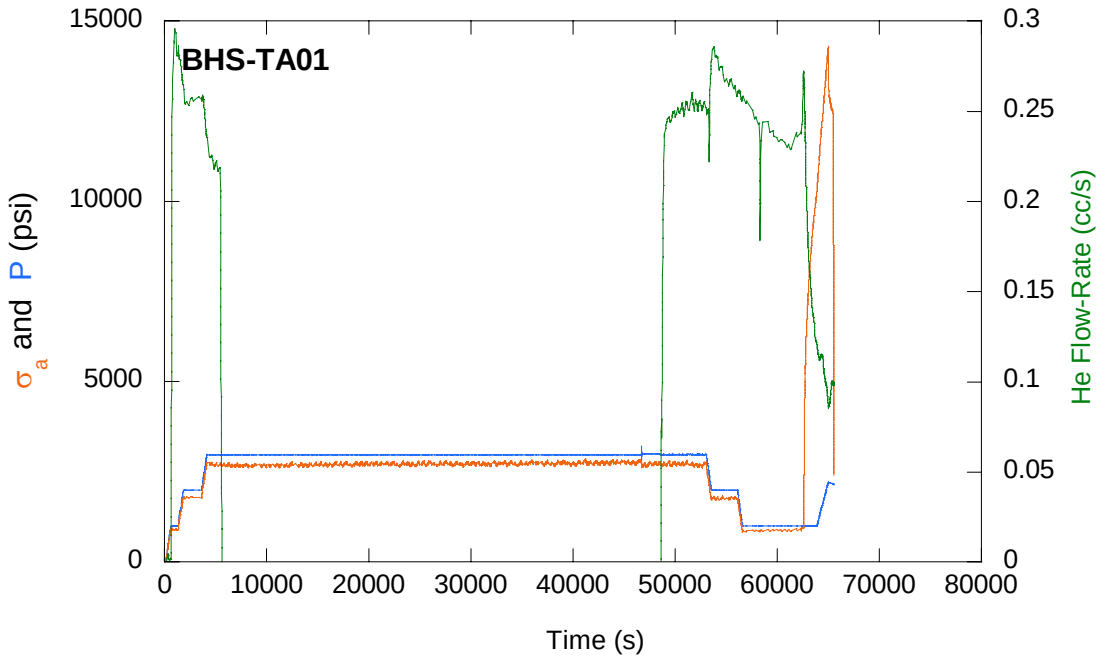
BHS-TA01
15000
10000
5000
0
0.3
0.25
0.2
0.15
0.1
0.05
0
0
10000
20000
30000
40000
50000
60000
70000
80000
Time (s)
σa and P (psi)
He Flow-Rate (cc/s)

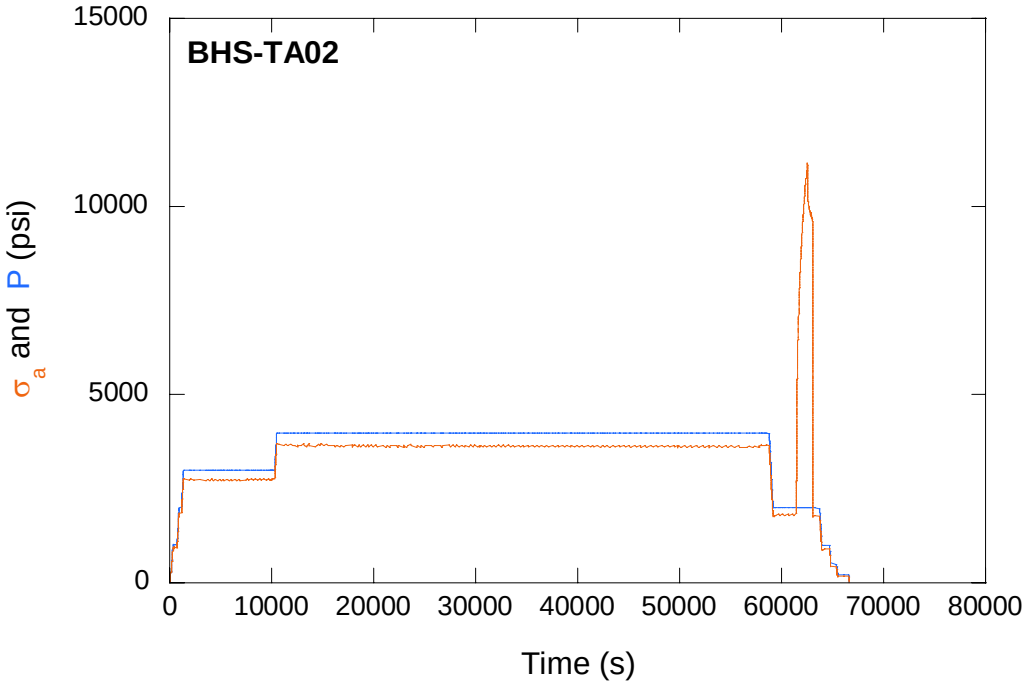
BHS-TA02
15000
10000
5000
0
0
10000
20000
30000
40000
50000
60000
70000
80000
Time (s)
σa and P (psi)

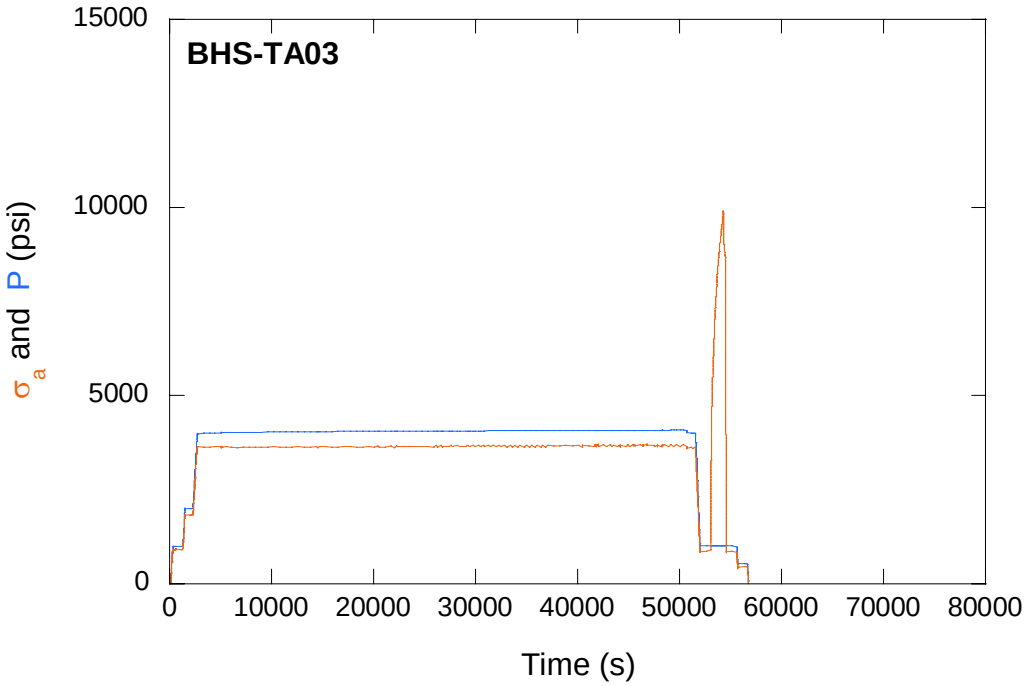
BHS-TA03
15000
10000
5000
0
σa and P (psi)
0
10000
20000
30000
40000
50000
60000
70000
80000
Time (s)

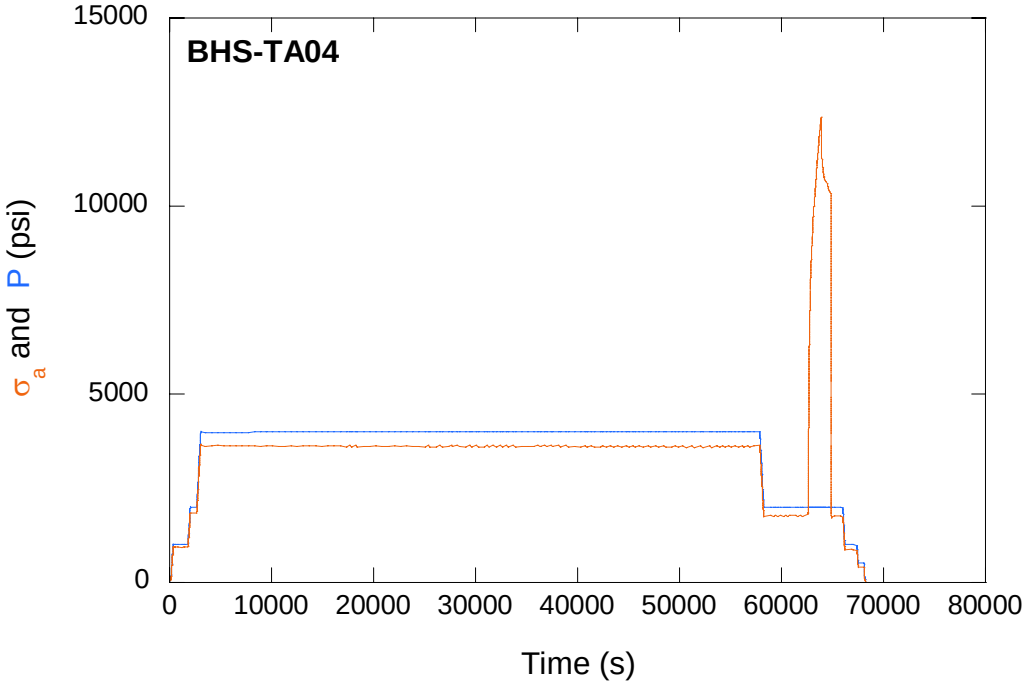
BHS-TA04
15000
10000
5000
0
σa and P (psi)
0
10000
20000
30000
40000
50000
60000
70000
80000
Time (s)

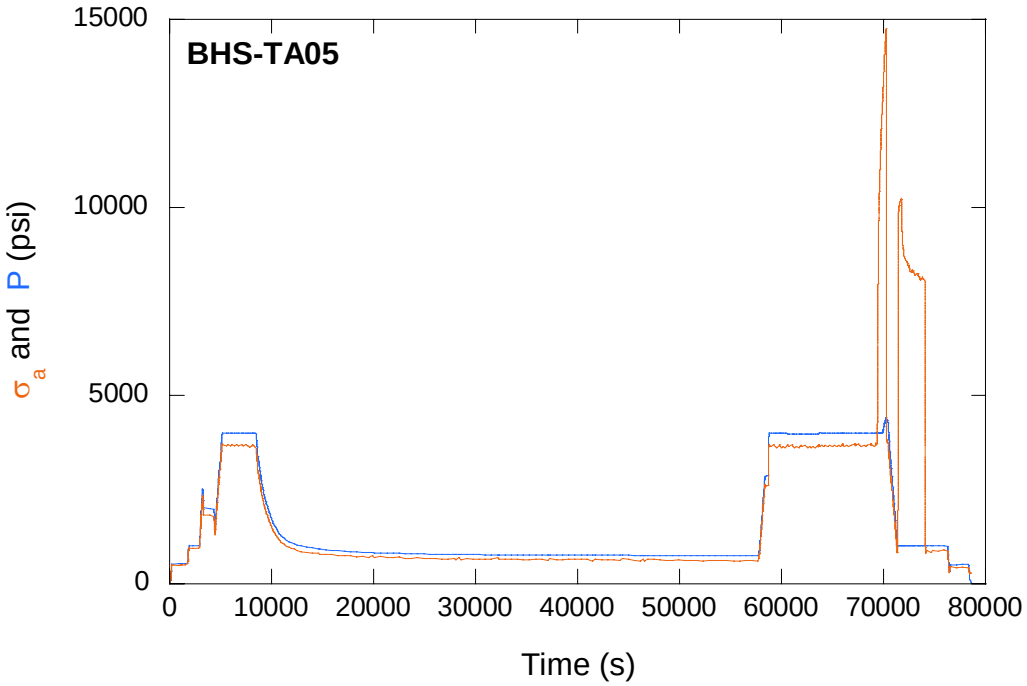
BHS-TA05
15000
10000
5000
0
σa and P (psi)
0
10000
20000
30000
40000
50000
60000
70000
80000
Time (s)

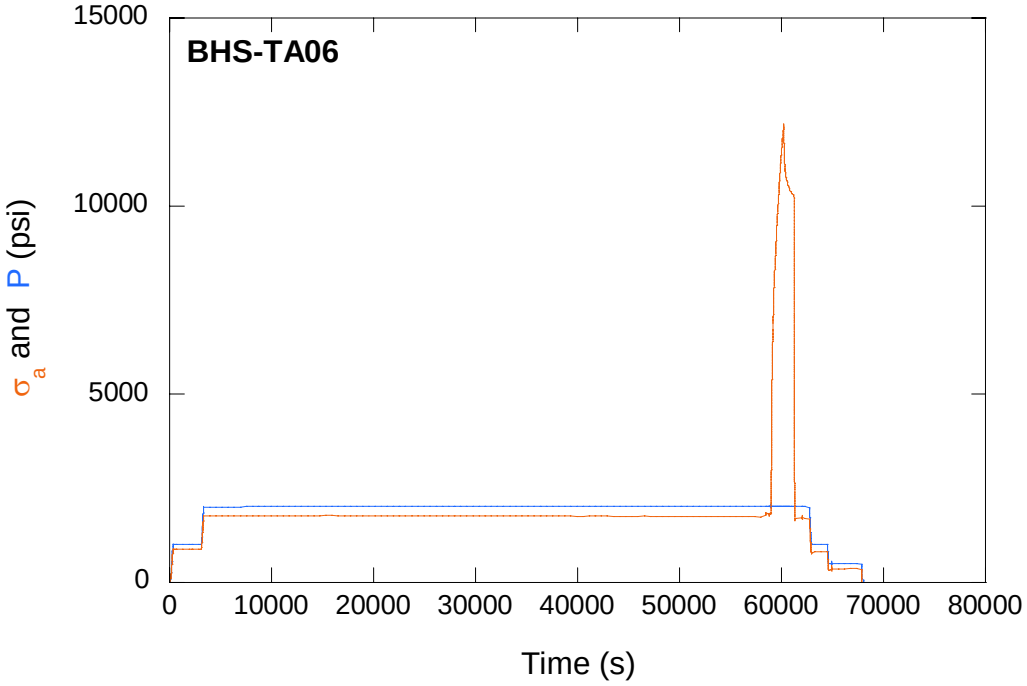
BHS-TA06
15000
10000
5000
0
σa and P (psi)
0
10000
20000
30000
40000
50000
60000
70000
80000
Time (s)

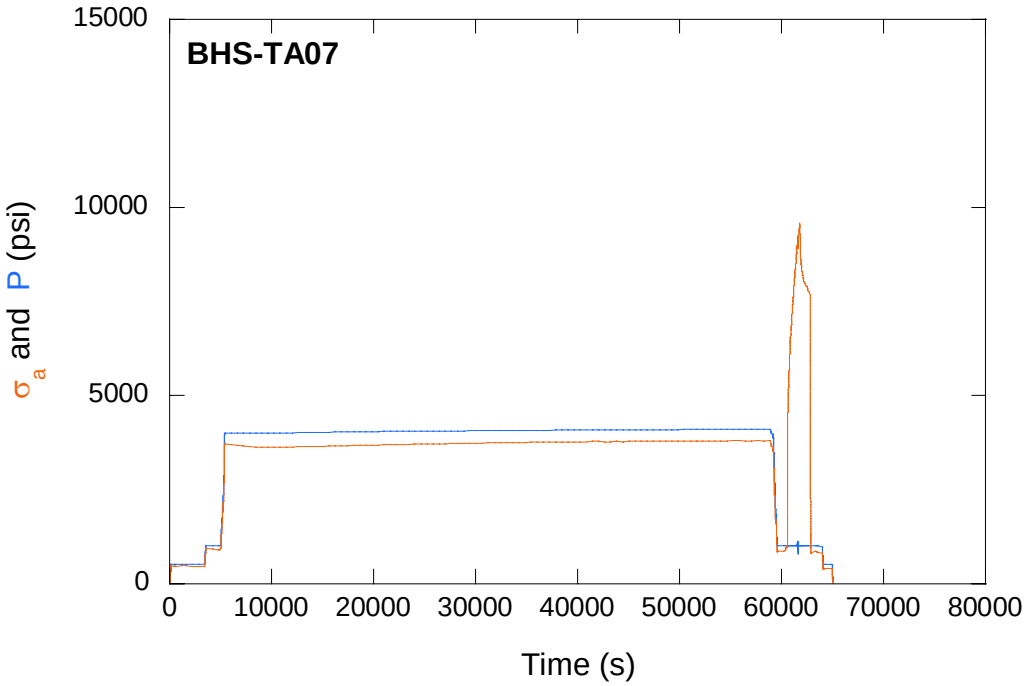
BHS-TA07
15000
10000
5000
0
σa and P (psi)
0
10000
20000
30000
40000
50000
60000
70000
80000
Time (s)

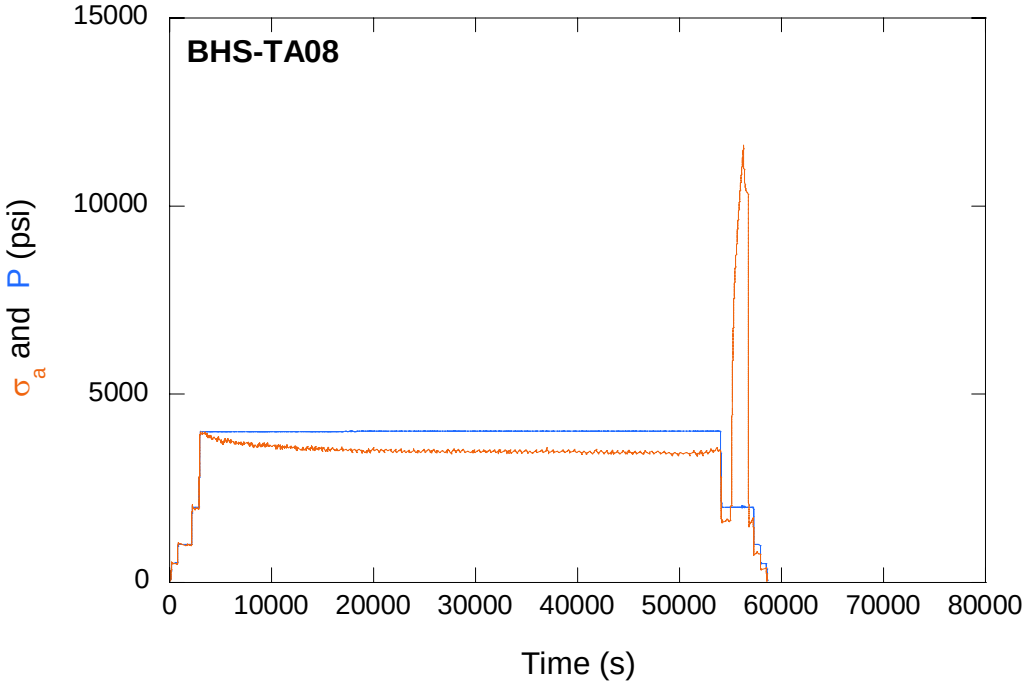
BHS-TA08
15000
10000
5000
0
σa and P (psi)
0
10000
20000
30000
40000
50000
60000
70000
80000
Time (s)

APPENDIX B

Stress-Strain Plots from Triaxial Compression Tests of Big Hill Salt

(σ_a-axial stress, ε_a-axial strain, ε_l-lateral strain, ε_v-volumetric strain, and P-confining pressure)

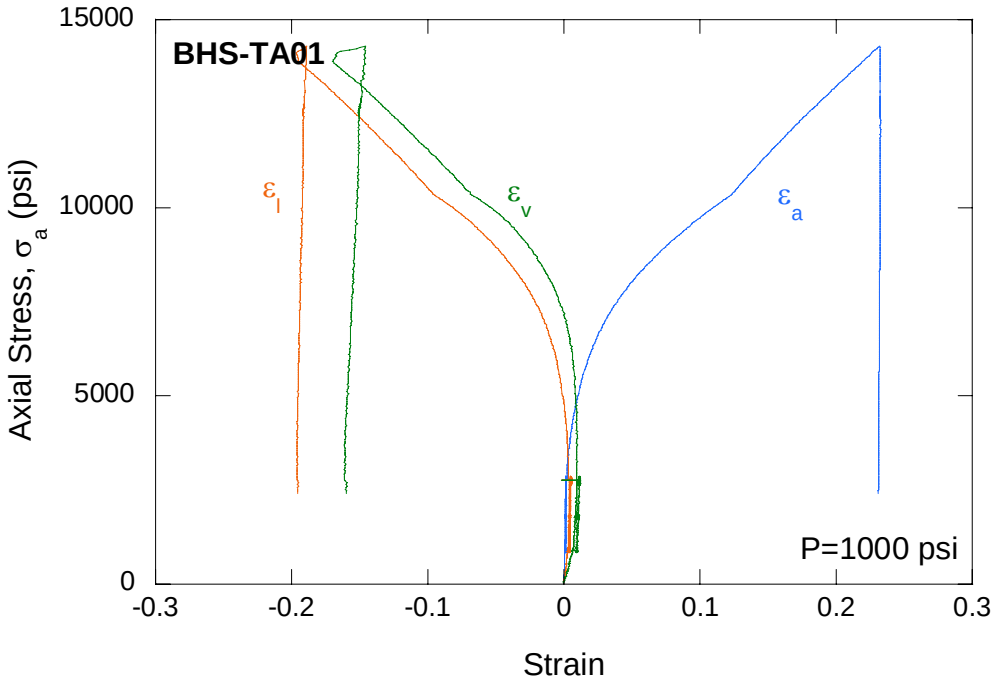
BHS-TA01
15000
10000
5000
0
Axial Stress, σa (psi)
εl
εv
εa
P=1000 psi
-0.3
-0.2
-0.1
0
0.1
0.2
0.3
Strain

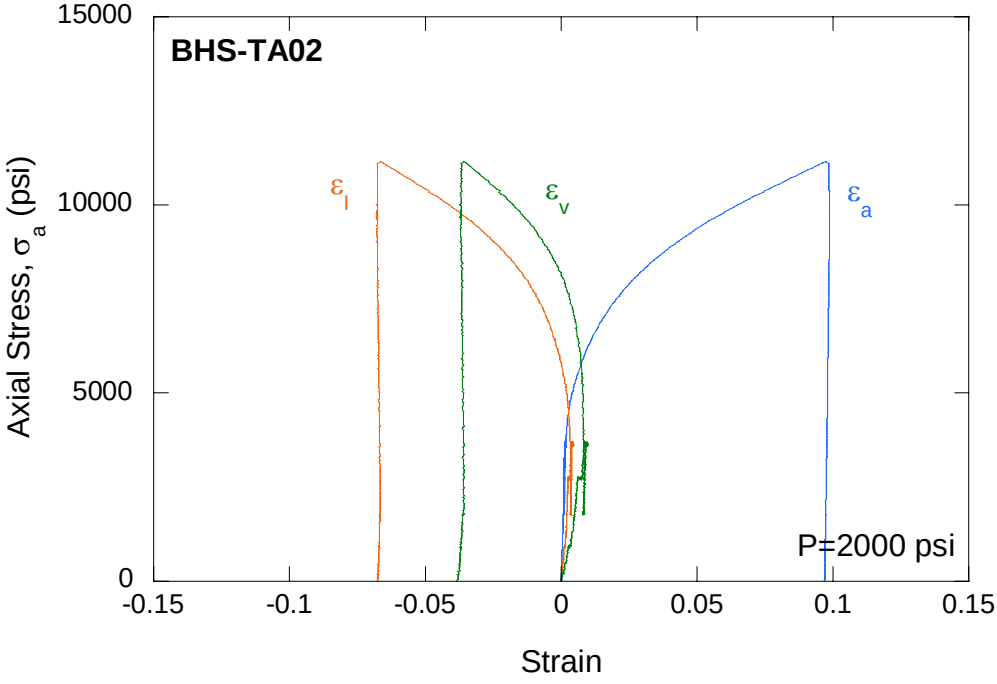
BHS-TA02
15000
10000
5000
0
Axial Stress, σa (psi)
εl
εv
εa
P=2000 psi
-0.15
-0.1
-0.05
0
0.05
0.1
0.15
Strain

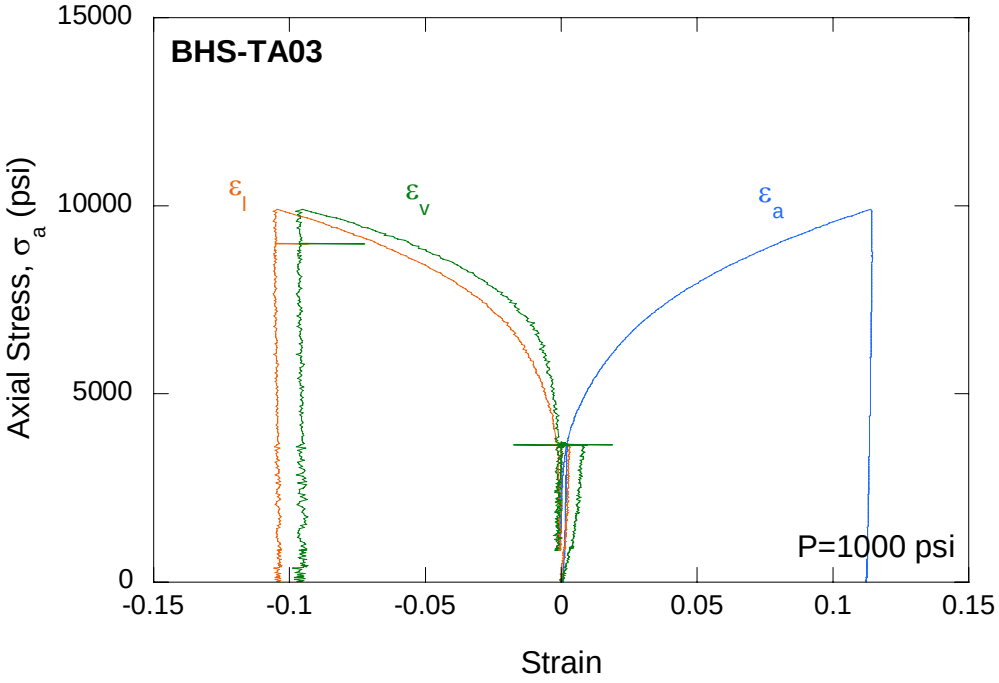
BHS-TA03
15000
10000
5000
0
Axial Stress, σa (psi)
εl
εv
εa
P=1000 psi
-0.15
-0.1
-0.05
0
0.05
0.1
0.15
Strain

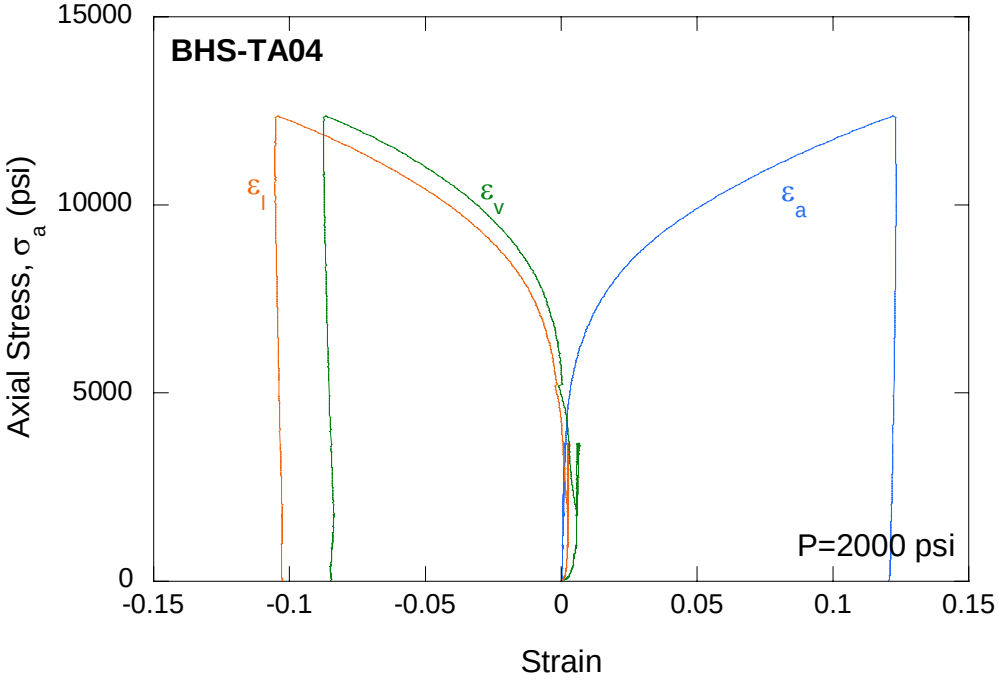
BHS-TA04
15000
10000
5000
0
Axial Stress, σa (psi)
εl
εv
εa
P=2000 psi
-0.15
-0.1
-0.05
0
0.05
0.1
0.15
Strain

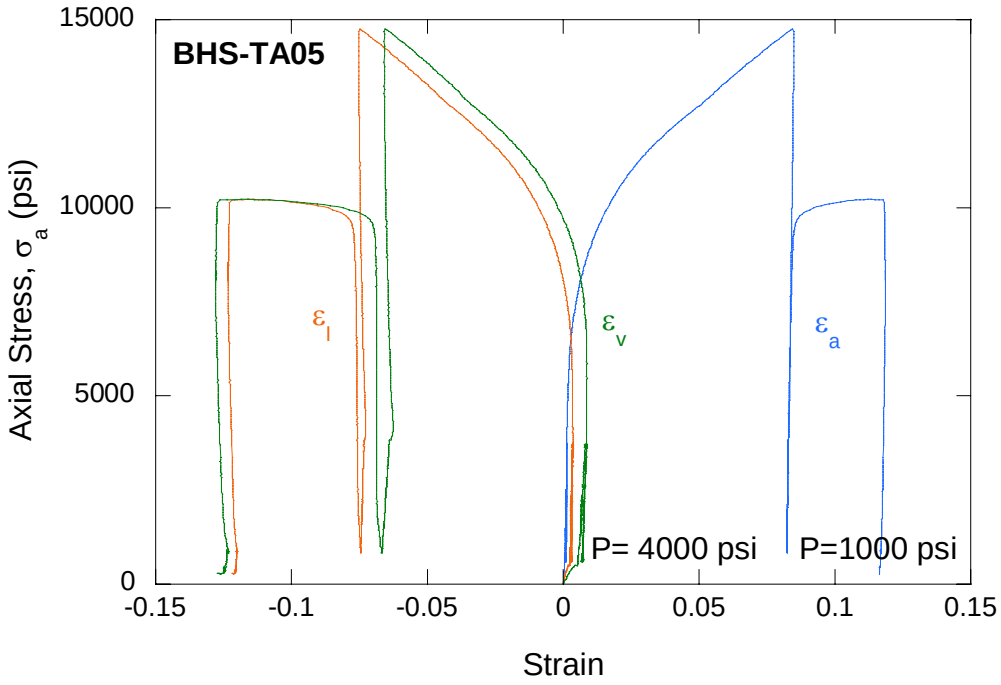
BHS-TA05
15000
10000
5000
0
Axial Stress, σa (psi)
-0.15
-0.1
-0.05
0
0.05
0.1
0.15
Strain
εl
εv
εa
P= 4000 psi
P=1000 psi

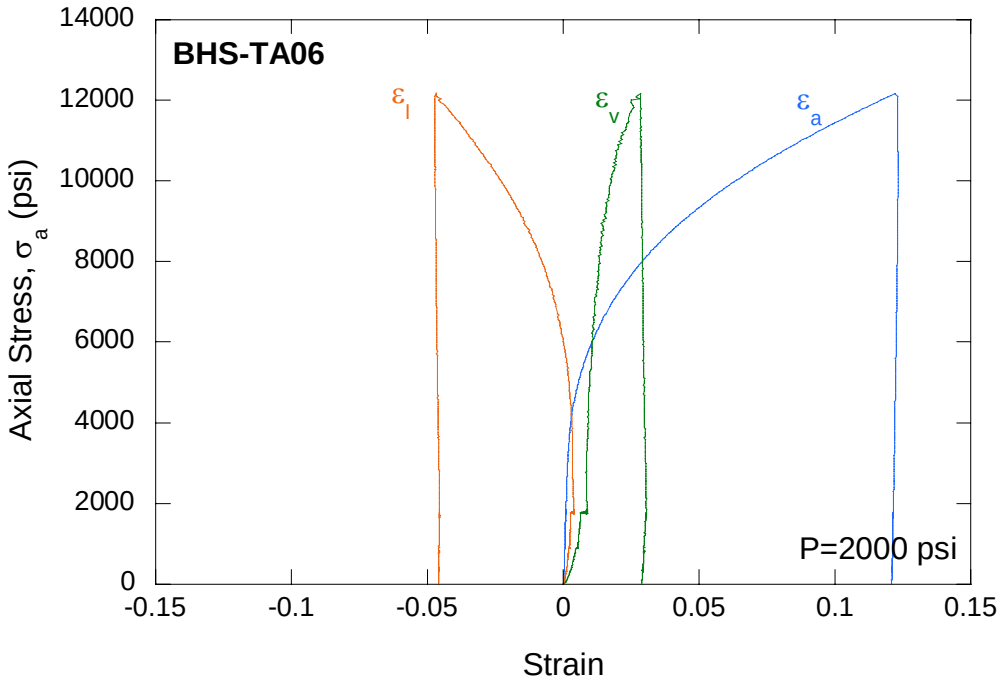
BHS-TA06
14000
12000
10000
8000
6000
4000
2000
0
Axial Stress, σa (psi)
-0.15
-0.1
-0.05
0
0.05
0.1
0.15
Strain
εl
εv
εa
P=2000 psi

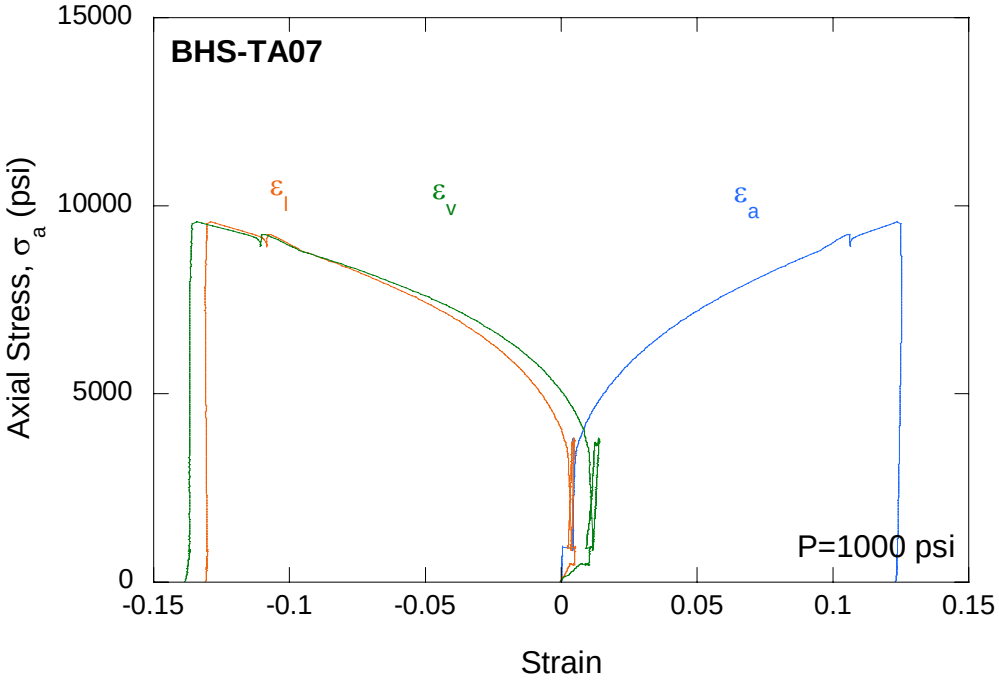
BHS-TA07
15000
10000
5000
0
Axial Stress, σa (psi)
εl
εv
εa
P=1000 psi
-0.15
-0.1
-0.05
0
0.05
0.1
0.15
Strain

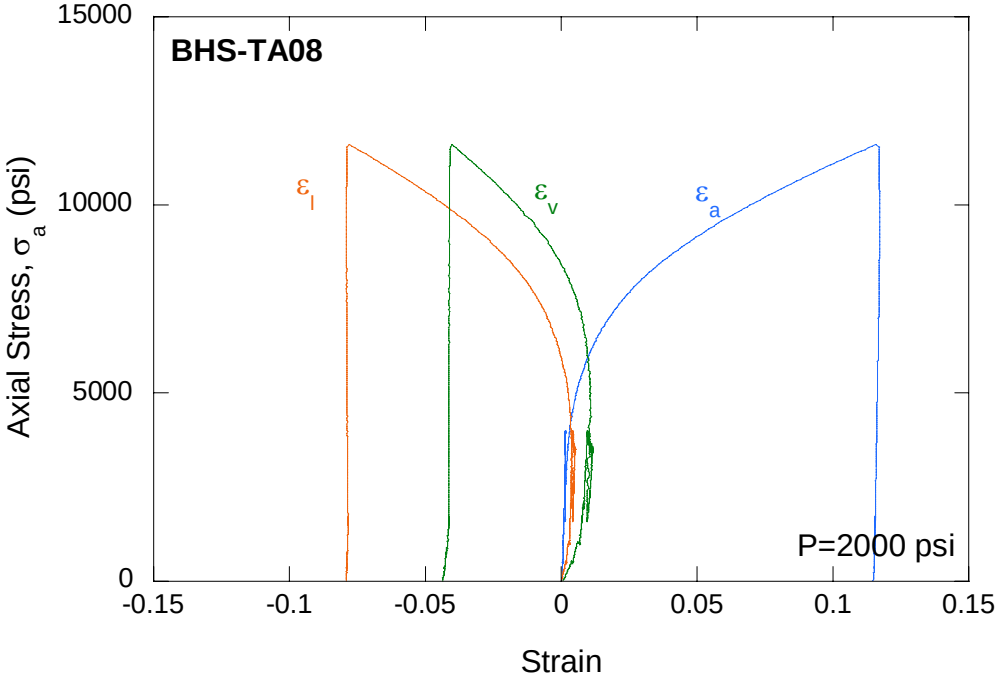
BHS-TA08
15000
10000
5000
0
Axial Stress, σa (psi)
εl
εv
εa
P=2000 psi
-0.15
-0.1
-0.05
0
0.05
0.1
0.15
Strain

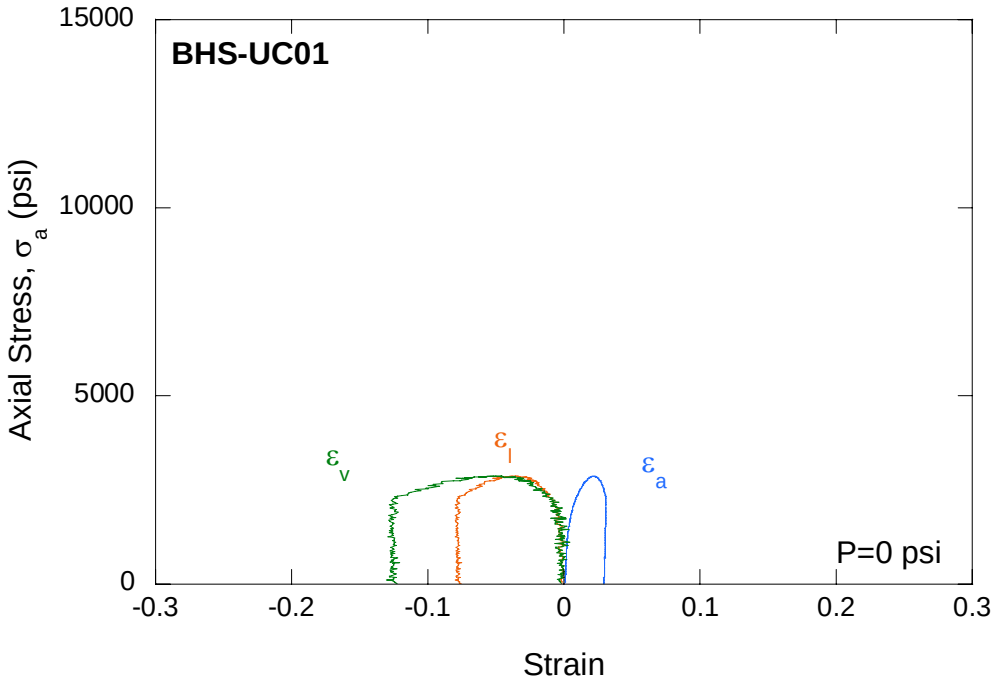
BHS-UC01
15000
10000
5000
0
Axial Stress, σa (psi)
-0.3
-0.2
-0.1
0
0.1
0.2
0.3
Strain
εv
εl
εa
P=0 psi

APPENDIX C

Stress-Strain Plots from Triaxial Compression Tests of Big Hill Salt for the Determination of Dilation Limit

(σ_a-axial stress, ε_a-axial strain, ε_l-lateral strain, ε_v-volumetric strain, and P-confining pressure)

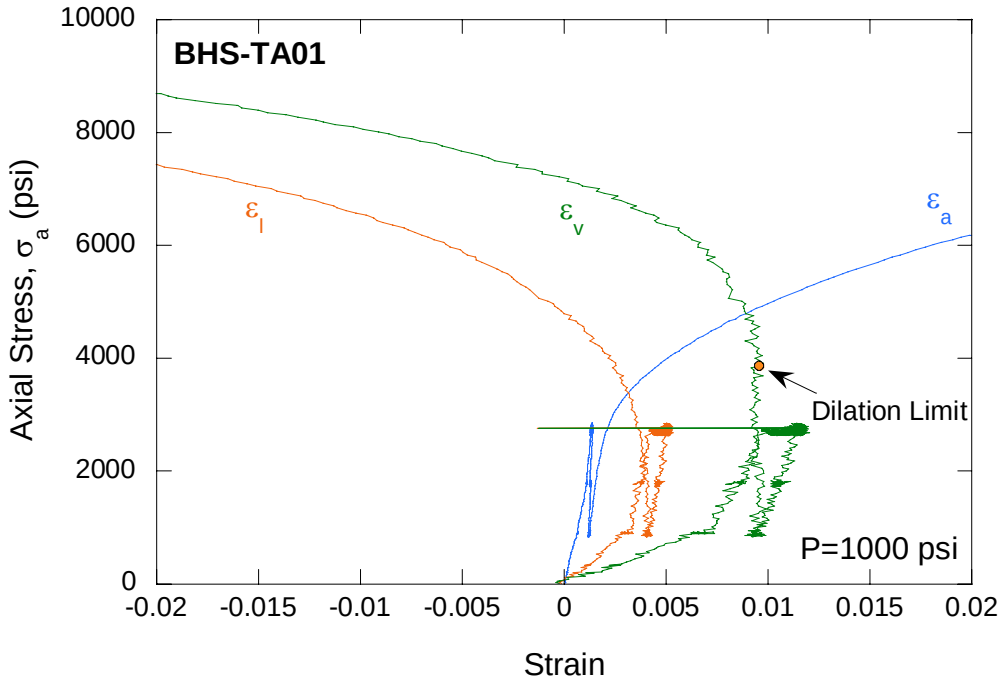
BHS-TA01
Axial Stress, σa (psi)
Strain
εl
εv
εa
Dilation Limit
P=1000 psi
10000
8000
6000
4000
2000
0
-0.02
-0.015
-0.01
-0.005
0
0.005
0.01
0.015
0.02

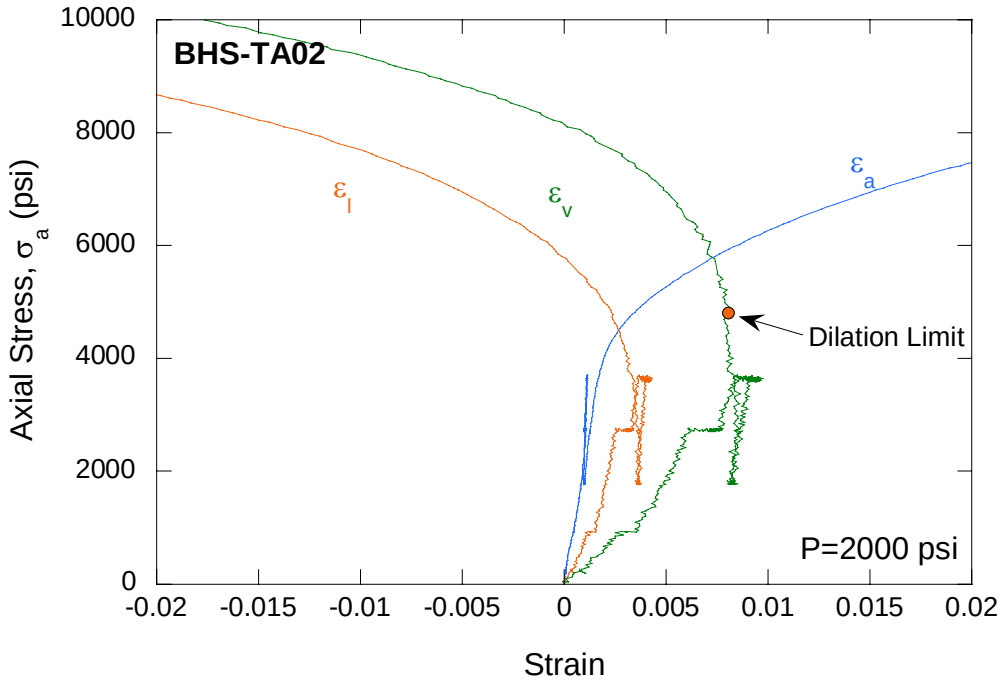
BHS-TA02
Axial Stress, σa (psi)
Strain
εl
εv
εa
Dilation Limit
P=2000 psi
10000
8000
6000
4000
2000
0
-0.02
-0.015
-0.01
-0.005
0
0.005
0.01
0.015
0.02

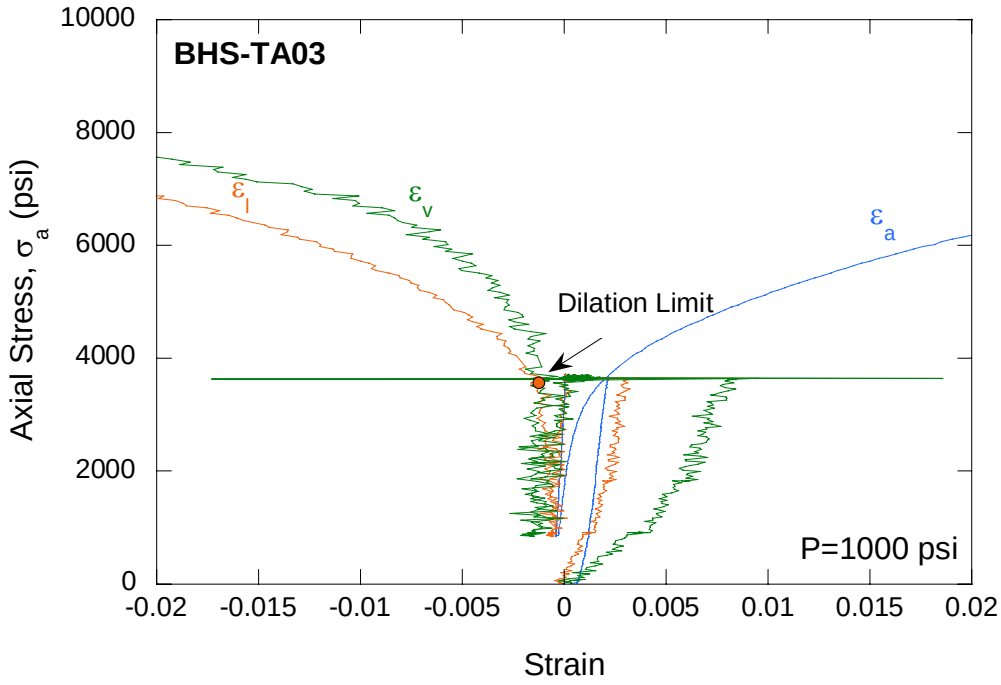
BHS-TA03
Axial Stress, σa (psi)
Strain
εl
εv
εa
Dilation Limit
P=1000 psi
10000
8000
6000
4000
2000
0
-0.02
-0.015
-0.01
-0.005
0
0.005
0.01
0.015
0.02

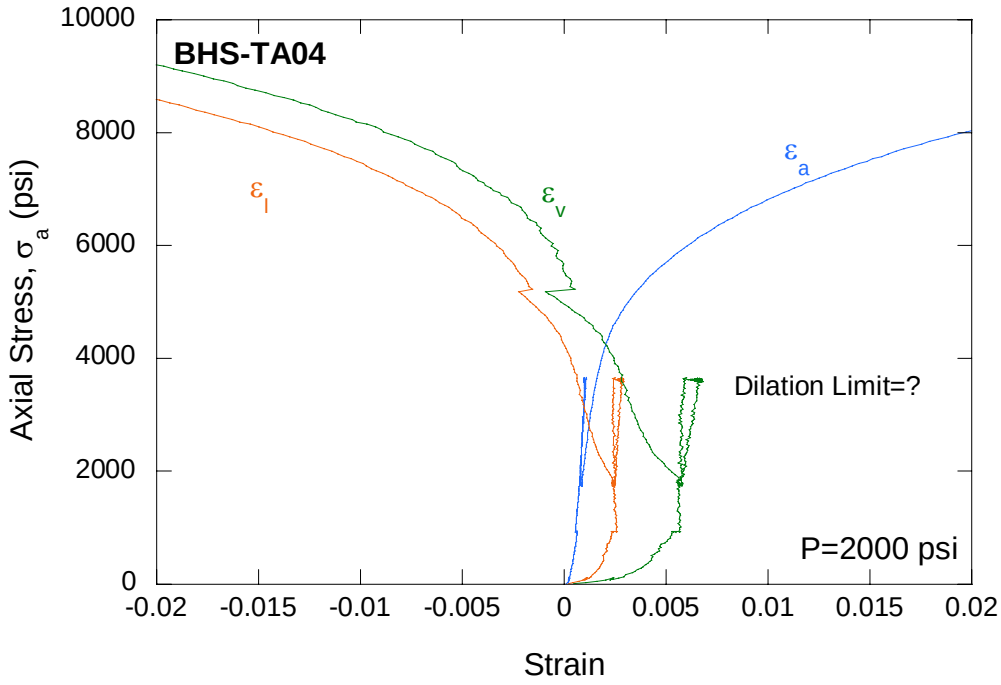
BHS-TA04
Axial Stress, σa (psi)
Strain
εl
εv
εa
Dilation Limit=?
P=2000 psi
10000
8000
6000
4000
2000
0
-0.02
-0.015
-0.01
-0.005
0
0.005
0.01
0.015
0.02

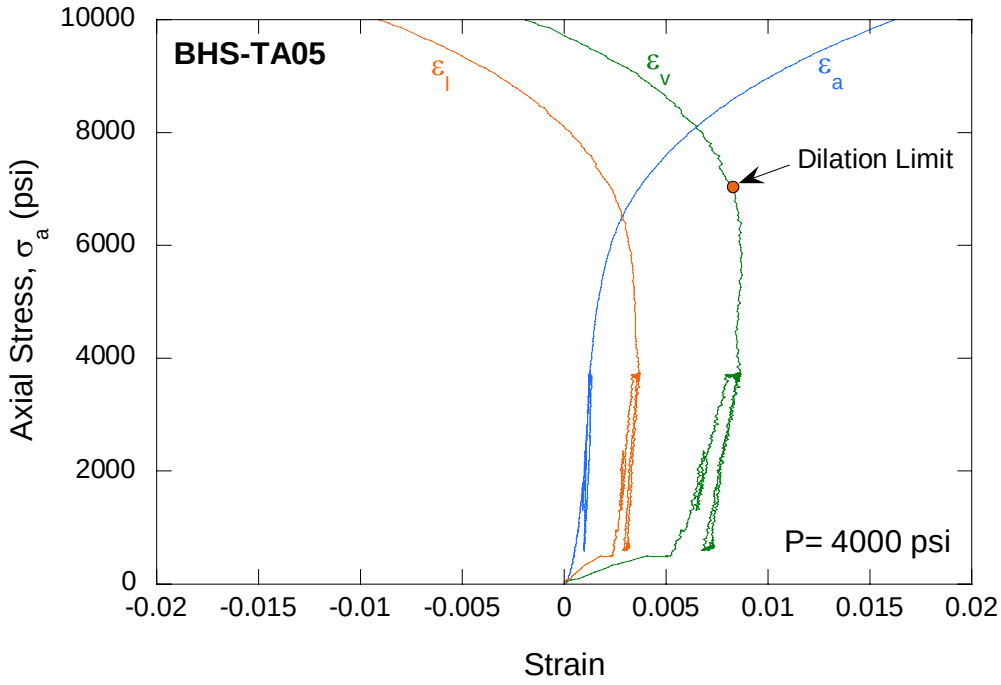
BHS-TA05
ε_l
ε_v
ε_a
Dilation Limit
P= 4000 psi
Axial Stress, σ_a (psi)
Strain
10000
8000
6000
4000
2000
0
-0.02
-0.015
-0.01
-0.005
0
0.005
0.01
0.015
0.02

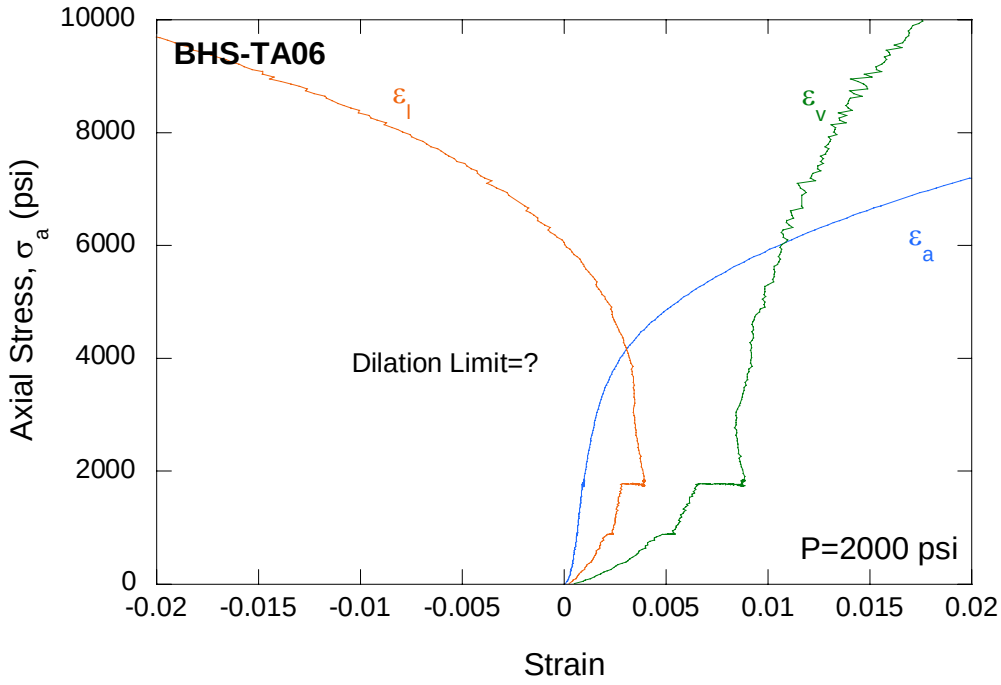
BHS-TA06
ε_l
ε_v
ε_a
Dilation Limit=?
P=2000 psi
Axial Stress, σ_a (psi)
Strain
10000
8000
6000
4000
2000
0
-0.02
-0.015
-0.01
-0.005
0
0.005
0.01
0.015
0.02

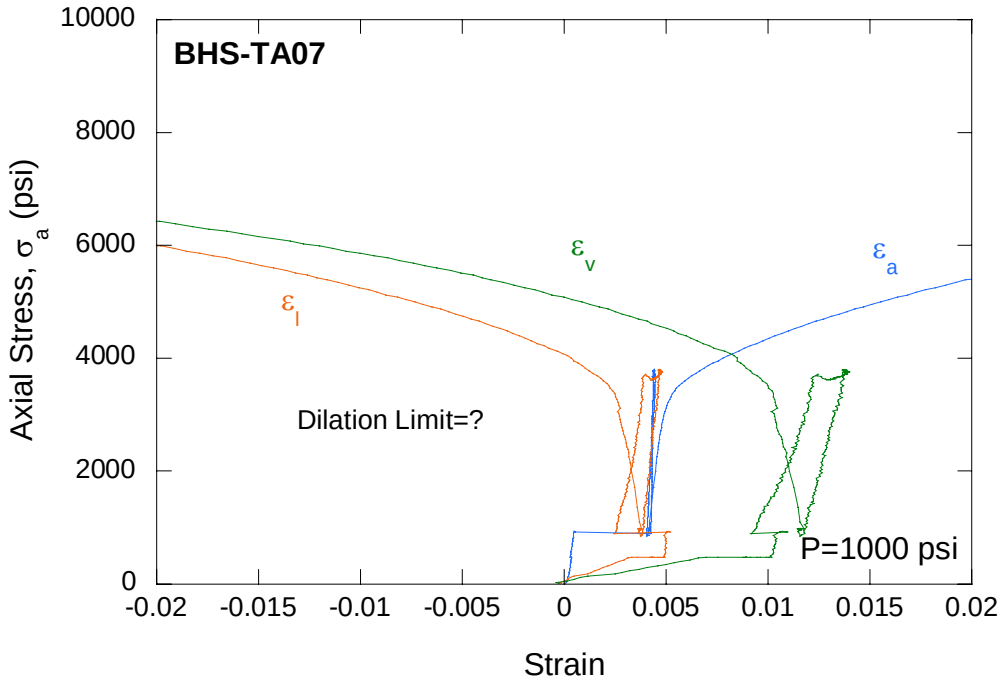
BHS-TA07
Axial Stress, σa (psi)
Strain
εv
εa
εl
Dilation Limit=?
P=1000 psi
10000
8000
6000
4000
2000
0
-0.02
-0.015
-0.01
-0.005
0
0.005
0.01
0.015
0.02

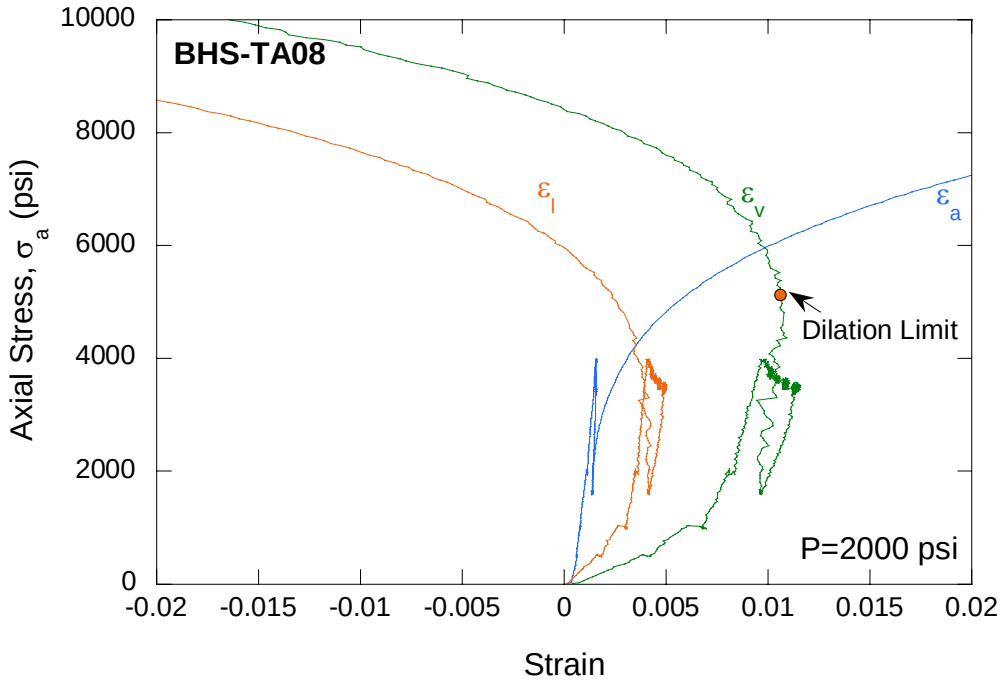
BHS-TA08
Axial Stress, σa (psi)
Strain
εl
εv
εa
Dilation Limit
P=2000 psi
10000
8000
6000
4000
2000
0
-0.02
-0.015
-0.01
-0.005
0
0.005
0.01
0.015
0.02

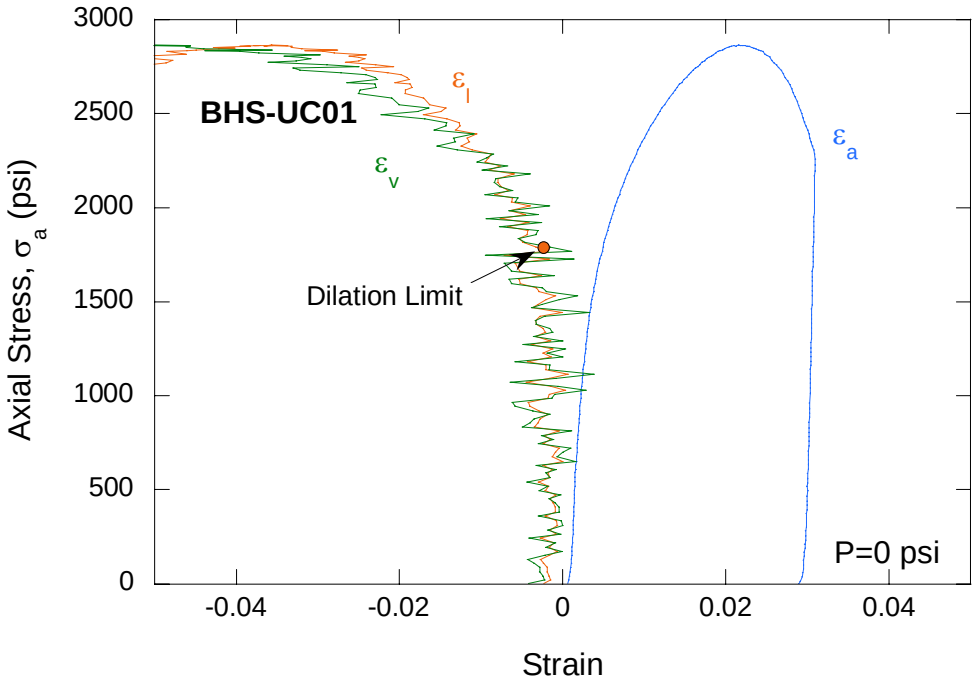
BHS-UC01
ε_l
ε_v
ε_a
Dilation Limit
P=0 psi
Axial Stress, σ_a (psi)
Strain
3000
2500
2000
1500
1000
500
0
-0.04
-0.02
0
0.02
0.04

APPENDIX D

List of Data and Supplemental Files Archived in Webfileshare System

List of files archived in the WEBFILESHARE system (https://wfsprod01.sandia.gov).

Folder Name	File Name	Description
/TARGET/Big Hill	Big-Hill-Sand2004.doc	This SAND report
/TARGET/Big Hill	Big Hill Salt Test Programrev3.doc	Test plan for damage criteria of Big Hill salt
/TARGET/Big Hill	Big Hill-master.xls	Master data file consists of the following five worksheets: **Test matrix**: Big Hill salt test matrix and core inventory **Triaxial data**: Test data from triaxial compression tests **Damage analysis:** Dilatant damage analyses in terms of stress invariants and principal stresses. **Permeability:** Test data from permeability measurements **Pictures:** Pictures of test set-up and selected specimens
/TARGET/Big Hill	Big Hill-Data-Sheets.zip	Laboratory data sheets consisting of original notes during testing.
/TARGET/Big Hill	Big Hill test raw data.zip	Raw data from triaxial/uniaxial compression tests of Big Hill salt
/TARGET/Big Hill	Big Hill-Pictures.zip	Miscellaneous pictures taken during triaxial compression testing of Big Hill salt
/TARGET/Big Hill	Big_hill_conversion.txt	Conversion equations used to obtain stress-strain data

DISTRIBUTION

Sandia National Laboratories
P.O. Box 5800
Albuquerque, NM 87185

DISTRIBUTION

1	MS 0701	P. J. Davies, 6100
1	MS 0701	J. A. Merson, 6102
1	MS 0706	D. J. Borns, 6113
5	MS 0706	B. L. Ehgartner, 6113
1	MS 0706	D. L. Lord, 6113
1	MS 0706	D. E. Munson, 6113
1	MS 0706	C. C. Rautman, 6113
1	MS 0706	A. R. Sattler, 6113
1	MS 0735	R. E. Finley, 6115
1	MS 0741	M. L. Tatro, 6200
1	MS 0750	T. E. Hinkebein, 6118
1	MS 0751	L. S. Costin, 6117
5	MS 0751	M. Y. Lee, 6117
1	MS 0751	T. W. Pfeifle, 6117
1	MS 1031	D. R. Bronowski, 6117
1	MS 1089	F. B. Nimick, 6101
5	MS 1395	B. Y. Park, 6821
1	MS 9018	Central Tech. Files, 8945-1
2	MS 0899	Technical Library, 9616
2	MS 0731	823/Library, 6850

U.S. DOE SPR PMO
900 Commerce Road East
New Orleans, LA 70123

1	W. C. Gibson, FE 44
4	W.S. Elias, FE-4431
1	R. E. Myers, FE 4421
2	TDCS

U.S. Department of Energy
Strategic Petroleum Reserve
1000 Independence Avenue SW
Washington, D.C. 20585

1	D. Johnson, FE 421

DynMcDermott
850 South Clearview Parkway
New Orleans, LA 70123
1 J. A. Farquhar, DM 21
1 J. M. McHenry. DM-21